EXPERIMENTAL INVESTIGATION OF EFFECT OF RESIDUAL STRESSES ON FATIGUE CRACK GROWTH IN PIPELINES WITH ALLOWANCE FOR THE SCALE EFFECTS

Delft University of Technology

Master Thesis

Adarsh Gupta

Student Number : 4243811

Faculty of Maritime, Mechanical and Materials Engineering
Department of Offshore and Dredging Engineering
Delft University of Technology
The Netherlands

2014

EXPERIMENTAL INVESTIGATION OF EFFECT OF RESIDUAL STRESSES ON FATIGUE CRACK GROWTH IN PIPELINES WITH ALLOWANCE FOR THE SCALE EFFECTS

Author:

Adarsh Gupta
Student Number: 4243811
Year: 2013-2014

Graduation Committee:

Prof. Dr. ir. M.L. Kaminski	Delft University of Technology
Dr. ir. Michael Janssen	Delft University of Technology
Dr. ing. Arie Romeijn	Delft University of Technology
Dr. Bin Hu	Allseas Engineering B.V.
Ir. Paula Van Lieshout	Delft University of Technology

Delft University of Technology

Table Of Contents

ACKNOWLEDGEMENT

I would like to express my appreciation and thanks to my chair Prof. Mirek Kaminski, for his patience and excellent guidance he provided me during my thesis study. I would like to thank my advisor Dr. Arie Romeijn, who helped me execute and analyze experimental data in an ordered way . I am grateful to my daily supervisor, Dr. Bin Hu, who provided me the platform to carry out this research study. Without his assistance and dedicated involvement in every step throughout the process, this thesis would have never been accomplished. It was his constant motivation and support which helped me shape my thesis to this end.

I would like to thank Dr. Michael Janssen and Paula Van Lieshout for being a part of my graduation committee. In addition, a special thanks to Dr. Michael for taking out time for valuable discussions which added significant value to this work.

I am thankful to Dr. Liang Zhang and Zhaoxiang Chen for their support during my experimental work and ping pong sessions. I would like to thank Dr. Ton Riemslag and Hans for their help without which this experimental work would have been difficult.

I would like to thank my friends Nishchay, Siddarth and Rishab who supported me in writing and incented me to strive towards my goal.

Lastly, I would like to thank my parents and brother who always supported my decisions and helped me in every possible way.

LIST OF SYMBOLS

Symbols

Latin Symbols

a	Crack depth parameter
Δa	Change in crack length
B	Thickness of pipe specimen
c	Crack/notch length parameter
C	Material constant
F	Applied force
h	Crack height
K	Stress intensity factor
K_r	Residual stress intensity factor
K_{max}	Maximum stress intensity factor
K_{min}	Minimum stress intensity factor
K_c	Critical stress intensity factor
ΔK	Stress intensity factor range
ΔK_{eff}	Effective stress intensity factor range
m	Slope of material
N	Cycle number
T	Time
R	Stress ratio
R_{eff}	Effective stress ratio
S_R	Applied static stress
Y	Geometry factor

Greek Symbols

$\Delta\sigma$	Stress range
$\Delta\sigma_m$	Membrane stress
$\Delta\sigma_b$	Bending stress
σ_L	Load stress
σ_a	Stress amplitude
σ_{max}	Maximum stress
σ_{min}	Minimum stress
σ_m	Mean stress

1 PROBLEM ANALYSIS

In the offshore industry, subsea pipelines are used for transporting oil and gas from oil/gas wells to remote platforms and from platforms to nearby shores. These pipelines are laid mostly using S-lay and J-lay methods. During their lifetime (installation and operation), these pipelines are subjected to huge cyclic stresses. Some loads which result in these cyclic stresses are reeling-on, reeling-off, bending over the aligner, straightening and the bending profile generated during laying during installation period. During operation phase, cyclic loads which may generate cyclic stresses include internal pressure variations, wave action and pipe vibration, such as that induced by vortex shedding [1]. These cyclic stresses are usually below the yield strength of the pipe material but play an important role during the lifetime of pipeline due to fatigue characteristics of pipe material. According to EN 1993-1-9 [2], "Fatigue is the process of initiation and propagation of cracks through a structural part due to action of fluctuating stress". If the stresses generated are above a threshold value of fatigue stress range, a microscopic flaw in pipeline will grow normal to principal stress direction. In case, these microscopic flaws gradually grow into critical crack size, the pipe material will fail by fracture.

Fatigue characteristics of a material are directly governed by several factors like cyclic stress state, temperature, geometry of specimen, surface quality, material type, residual stresses, size & distribution of internal defects and grain size of material. Among these factors, the common defect encountered in subsea pipelines is the notch which may arise during welding process. These notches can act as initiation points for cracks in pipes. It is important to monitor the size of these notches and to compromise the pipe if the notch size is greater than the critical notch size. The code BS 7910:2005 [3] gives the lower bound for crack growth rates based on past experiences with offshore structures. These values are usually overly conservative as these are given for a general set of temperature, material property and environmental conditions. So, there is a need to find an alternative to set the lower bound of crack growth rates for individual cases to optimise the design while ensuring the integrity of the system. One such alternative method is to carry out the destructive testing of strip specimens from the full scale pipe and find the crack growth rate for the given cyclic loading conditions. It is required to compare the crack propagation rate between the strip specimen and the pipe specimen.

Welding of steel pipes is a complex phenomenon and gives rise to residual stresses and distortions. Residual stresses are generated in the vicinity of weld seam during welding process which, if tensile, can be detrimental to fatigue strength of the pipes. During welding, a very complex thermal cycle is applied to the weldment which in turn causes irreversible elastic-plastic deformations and gives rise to the residual stresses in and around fusion zone and heat affected zone during cooling process among the several effects (like change in microstructure, rough surface profile), it produce in the weld area [4]. The influence of these residual stresses on fatigue strength of steel pipes remain an area of interest and there is a need to investigate its effects on fatigue strength exclusively.

2 INTRODUCTION

2.1 Fatigue

“Fatigue or fatigue damage refers to the modification of the properties of materials due to application of stress cycles whose repetition can lead to failure" [5].

Fatigue life of a structure is divided into three stages :

Crack initiation or nucleation: Crack initiation or micro-cracks are initiated due to cyclic plastic deformation under cyclic loading. The number of cycles for crack initiation depends on the condition of the material. In the presence of stress concentrators like notch defect, crack initiation can occur under small number of loading cycles.

Stable crack growth: In this phase, the micro-cracks propagate and join to form a propagating crack growing perpendicular to principal tensile stress in a stable manner. The crack surface can be characterised by the presence of beachmarks. The beachmarks on crack surface are quite visible if material is subjected to variable amplitude loading.

Unstable crack growth: In this phase, crack increases to a size at which the stresses generated on the reduced cross section area of the material exceeds the tensile strength of material or the stress intensity factor range reaches critical stress intensity factor range. The crack then starts growing at an exponential rate until the fracture of component takes place.

2.2 Crack Growth Model

Fatigue crack growth rate remains the area of interest and was investigated by many researchers in the past. Fatigue crack growth can be divided into three stages as shown in Figure 1. Stage-I is the crack initiation period in which crack growth rate is of the order of 10^{-6} mm/cycle. The crack growth in this region is mainly governed by micro structure features like grain size, applied stress intensity factor range, temperature and environmental conditions. Microstructure, mean stress and environment have a large influence in this region.

Many theories have been proposed for calculation of crack growth behaviour in stage II. Predominant among them is the Paris law given by Paris (et al) in 1961 [6] for crack growth rate in region II as follows:

$$\frac{da}{dN} = C\Delta K^m \qquad \text{Equation 1}$$

where C and m are material constants that are determined empirically. According to this law, crack growth rate (da/dN) is a function of stress intensity factor range. The main limitation of this law is that it does not consider the effect of stress ratio on the crack propagation behaviour. The crack growth rate according to this model can be described by the linear region (stage II) in the log-log plot in Figure-1. The crack growth rate is of the order of 10^{-5} mm/cycle to 10^{-2} mm/cycle in this region.

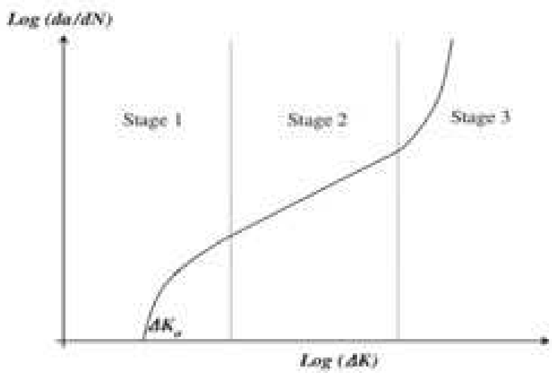

Figure 1:Typical fatigue crack growth behaviour in metals

In welded materials, the stress ratio ($\sigma_{min}/\sigma_{max}$) and mean stress ($\sigma_m$) is increased due to the presence of residual stresses generated during welding. The effect of increase in stress ratio needs to be considered while studying the effect of residual stress on fatigue strength. Forman's law considers the effect of stress ratio on crack growth rate and has the form [7]:

$$\frac{da}{dN} = \frac{C(\Delta K)^m}{(1-R_{eff})K_c - \Delta K} \qquad \text{Equation 2}$$

where K_c is the stress intensity factor when crack growth rate becomes unstable(critical), N is number of loading cycles, ΔK is the stress intensity factor range, C and m are experimentally determined constants and effective stress ratio (R_{eff}) is given by

$$R_{eff} = \frac{K^{\sigma}{}_{\min} + K_r}{K^{\sigma}{}_{\max} + K_r} = \frac{K^{\min}{}_{eff}}{K^{\max}{}_{eff}} \qquad \text{Equation 3}$$

where $K^{\sigma}{}_{\min}$ and $K^{\sigma}{}_{\max}$ are stress intensity factors at minimum and maximum loads respectively and K_r represents the stress intensity factor due to residual stress in the weld region.

2.3 Fatigue Parameters

A structure can be subjected to constant amplitude cyclic stresses or variable amplitude cyclic stresses during its service life. The simplest among them is the application of constant amplitude cyclic stresses shown in Figure 2 which is generally used in laboratories to carry out fatigue tests.

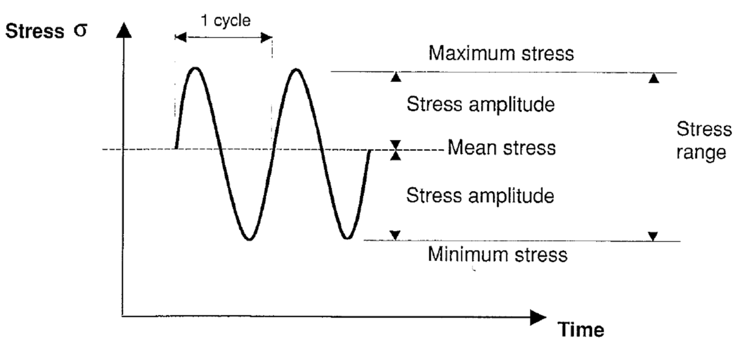

Figure 2 Constant Amplitude Stress History (Source: ECCS [8])

Some of the parameters related to the constant amplitude loading are defined below:

σ_{max} = maximum stress applied during loading cycle

σ_{min} = minimum stress applied during loading cycle

σ_m = mean stress = $(\sigma_{max} + \sigma_{min})/2$

σ_a = stress amplitude = $(\sigma_{max} - \sigma_{min})/2$

$\Delta\sigma$ = stress range = $\sigma_{max} - \sigma_{min} = 2.\ \sigma_a$

R = stress ratio = $\sigma_{min}/\ \sigma_{max}$

The mean stress (σ_m) has significant influence on the fatigue life of a structure. The fatigue life of a structure decreases with increase in applied mean stress during cyclic loading of structure [9]. Mean stress amplitude is dependent on both external loads applied and the residual tensile stresses present in structure which are generated during fabrication processes like welding, cutting, rolling, etc. The residual tensile stresses which are generated due to non-uniform plastic strains developed in structure during fabrication processes superimpose on the external load induced stresses and increase the magnitude of effective mean stress in that region. This phenomenon may lead to significant decrease in the fatigue strength of the structure, also known as residual stress effect. If the maximum stress due to superimposition of applied mean stress and residual tensile stress exceed the yield strength of the material, relaxation of residual tensile stress takes place and the maximum applied tensile stress is reduced to yield stress of material as shown in Figure 3.

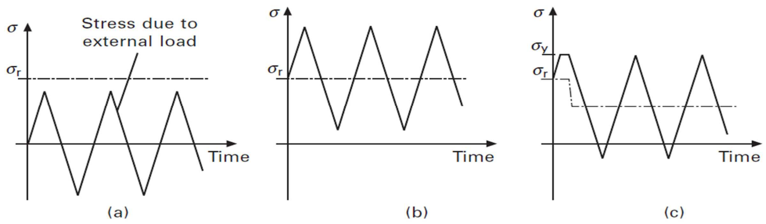

Figure 3 Effect of residual stresses on mean stress (Source : W. Fricke [10])

Geometrical factors play an important role in fatigue strength of a structure as well. Notches and cross-section variations are the points of stress concentrations in a structure where cracks can initiate by a small number of load cycles and at low nominal stress values. These notches can originate during the welding process as shown in Figure 4.

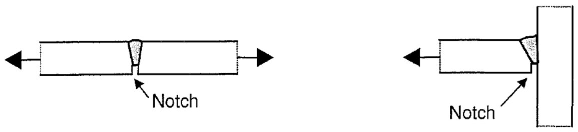

Figure 4 Notch in single side butt welds between two plates or hollow sections [Source: Ashby [11]]

In the presence of a notch, the lines of force tend to concentrate in the vicinity of the crack tip which leads to increase in stress concentration in notch region as shown in Figure 5.

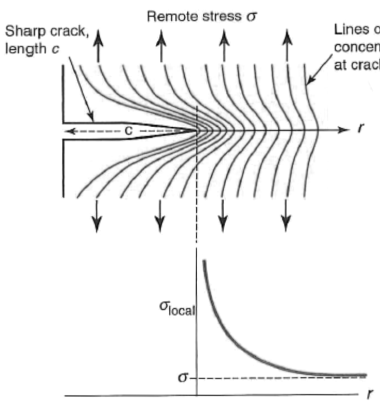

Figure 5 Figure shows stress concentration near notch region [Source: Ashby [11]]

2.4 Approaches For Fatigue Strength Assessment

Fatigue strength is defined as the stress level at which a corresponding number of cycles (N) will lead to failure (crack initiation). There are various approaches for the fatigue strength assessment of structures. They are broadly classified as global and local, based on the approach used to assess the fatigue strength. They are termed global approaches if they proceed directly from the external forces and moments or from the nominal stresses in the critical cross-section derived therefrom, under the assumption of a constant or linearised stress distribution [12]. The approaches are known as local if they consider local stress and local strains to assess the fatigue strength of structure. The different methods used to assess fatigue strength are shown in Figure 6.

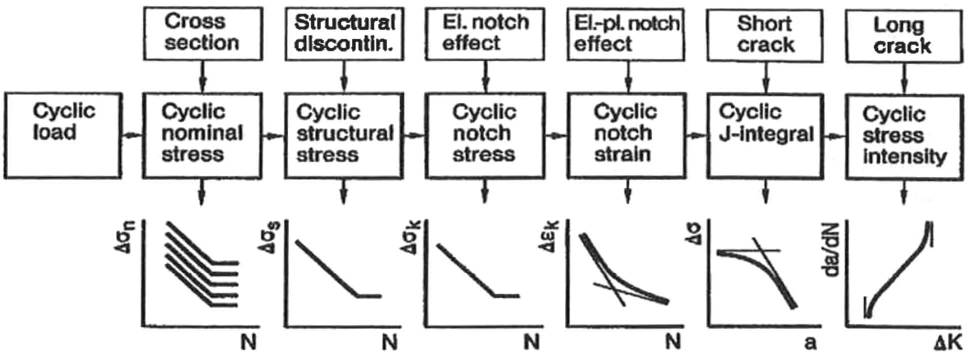

Figure 6 Fatigue Strength Assessment Methods [Source: D. Radaj [12]]

2.4.1 Nominal stress approach

In Nominal stress approach, the nominal stress generated (for non-welded members) from external loads and moments are calculated and then compared with nominal stress S-N curves. These members are classified into detail categories based on material, geometry (includes notch and size effect) and surface (includes hardening and residual stresses). The allowable stress ranges for each category is given in S-N curves for a specified number of loading cycles as shown in Figure 7.

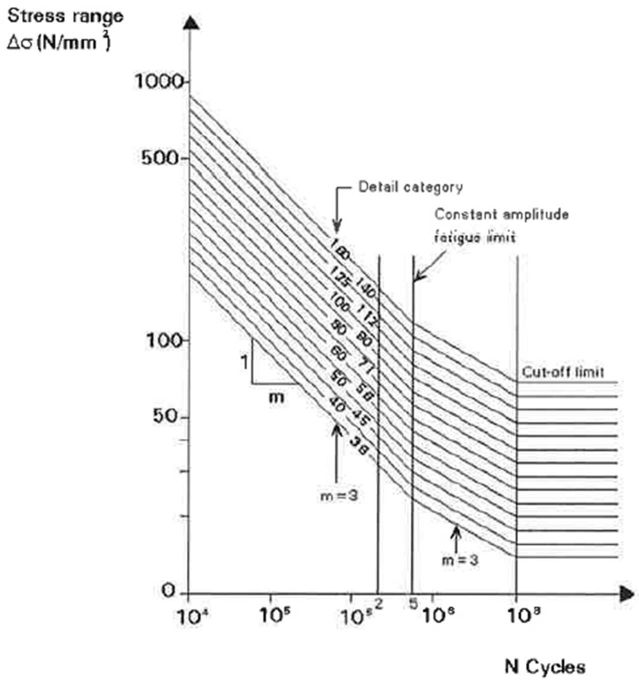

Figure 7 S-N Curves for different details categories [Source: ESDEP [13]]

2.4.2 Structural or hot spot stress approach

In this approach, the maximum stress at a region, also known as hot spot, is calculated. It is called hot spot as temperature rises in that particular region due to cyclic plastic deformation prior to crack initiation. This stress includes all the stress raisers except the non-linear stress increase due to notch effect as shown in Figure 8. The hot spot stress can be calculated by the finite element methods or by deformation measurements. The advantage of Structural hot spot stress approach is that it can be applied to the cases where the structure does not fall into standard nominal stress detail categories. The limitation of this method is that it can be applied to those detail types only where crack tends to initiate from the weld toe. It cannot be applied to cases where crack tend to initiate from weld root or internal defects as it will be difficult to determine hot spot stresses in these regions.

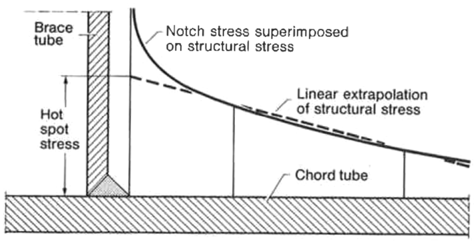

Figure 8 Hot spot stress at the weld toe of tubular joint, elimination of nonlinear rise in notch stress [Source: Wardenier [14]]

2.4.3 Notch stress approach

In Notch stress approach, both stress concentration and strength reduction by notches is taken into account during fatigue strength assessment of structure. This approach assumes that there is no appreciable plastic deformation at the notch root. The fatigue notch factor is derived by taking micro structural support hypothesis into account as discussed in Radaj [12]. The term 'micro structural support' means that maximum notch stress according to theory of elasticity is not decisive for crack initiation and propagation but instead some lower stress gained by averaging the maximum stress over a material characteristics small length, area or volume at the notch root (explicable from grain structure, micro yielding and crack initiation processes) [12]. The notch stress approach can be extended for finite fatigue life assessment by considering notch strain approach.

2.4.4 Notch strain approach

Notch strain approach was developed as an extension of notch stress approach to move from infinite fatigue life to finite fatigue life. It considers the effect of elastic-plastic strain at the notch root. The strength assessment consists in determining the stresses and strains in notch root in elastic plastic condition and comparing them with the strain S-N curve of material in the miniaturised specimen up to complete fracture or in a larger specimen up to technical crack initiation [12].

2.4.5 Crack propagation approach

This approach is used in damage tolerant design. It is mainly relevant to fatigue strength assessment of welded joints. There is significant probability of defects (notch, surface roughness) occurring in welded joints. Due to presence of these defects, crack initiation life in such structures is usually smaller than crack propagation life. Residual life assessment of a structure in these cases is done in the presence of inherent flaws to decide the acceptable service life of the structure under design cyclic stress ranges. Many empirical relations have been put forward for the calculation of crack propagation rate as a function of stress intensity factor range in structures. The most basic and simplest of them is the Paris law proposed by Paris and Erdogan [6]. Paris observed that the data from crack growth tests for a given material could be represented as a single graph if one plots the graph in log-log scale between crack growth rate (da/dN) and stress intensity factor range (ΔK). Based on empirical results, he formulated following relation (equation 1) between crack growth rate and stress intensity factor range.

$$\frac{da}{dN} = C\Delta K^{m}$$

$$\Delta K = \Delta\sigma * Y * \sqrt{(\pi * a)} \qquad \text{Equation 4}$$

The parameters which influence crack growth rate according to Paris law are:

ΔK - Stress intensity factor range

C - material constant

m - Slope, depends on material

Δσ - Stress range

Y - Geometry factor

a - crack length

2.5 Crack Growth Rate Measurement

In this research study, it is required to monitor crack growth rate of semi-elliptical crack on pipe surface in both the circumferential direction and along thickness direction. There are various destructive and non-destructive methods to monitor the crack growth rate. Some prominent methods are alternating current potential drop method and direct current potential drop method as discussed by L. Satyanarayan [15]. These methods can be used to measure through thickness crack lengths in combination with optical measurements. The optical measurements are used to make a calibration curve between potential drop data and crack lengths as required for further processing of potential drop data. It is, however, difficult to determine crack depth in case of surface cracks for opaque materials using optical methods. So, indirect methods like method of beachmarks can be employed to monitor crack depths [15] [16]. In this method, beachmarks are produced on fracture surface by varying the stress ranges applied during fatigue test. These beachmarks are used to relate the crack depth to crack length by using a calibration function. Direct current potential drop method can then be used to monitor crack growth in thickness direction as discussed by H.-M Bauschke (et al) [17].

The direct current potential drop method is prone to some errors which can be reduced to acceptable values using some measures as discussed by H.-M Bauschke (et al) [17]. Gage length(2y) as shown in Figure 9, affects the accuracy and sensitivity of the direct current potential difference method significantly. It is shown that the sensitivity of the potential difference measured increases with decrease in gage lengths, particularly for shallow surface cracks. The contribution of material on both sides of crack to potential difference change increase with increase in gage length, which is an added disadvantage.

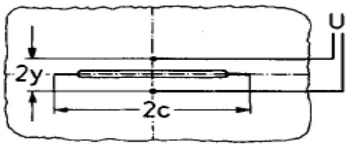

Figure 9 Figure shows the position(U) of potential probes in the vicinity of surface crack. 2y shows the distance between probes and 2c represents the crack length.(Source: H.-M Bauschke [17])

It is further noted that the shorter the gage length, smaller is the positioning errors of potential probes.

2.6 Fracture

It is local separation of a material or a structure into two or more parts under the action of stress. Irwin observed that there are three possible ways in which crack faces can move with respect to each other. These modes are termed as Mode I, Mode II and Mode III as shown in Figure 10.

Mode I: Mode I, also known as Opening mode, occur due to common mode of loading in which tensile stress acts normal to plane of crack. In this mode, displacement of the crack surfaces is perpendicular to plane of crack.

Mode II: Mode II is also known as in-plane shear mode or sliding mode. In this mode, crack surfaces move in the plane of crack and perpendicular to crack front as shown in Figure 10.

Mode III: In this mode, displacement of crack surfaces is in plane of the crack and parallel to the crack front. This mode is also known as Out of Plane Shear Mode or Tearing Mode.

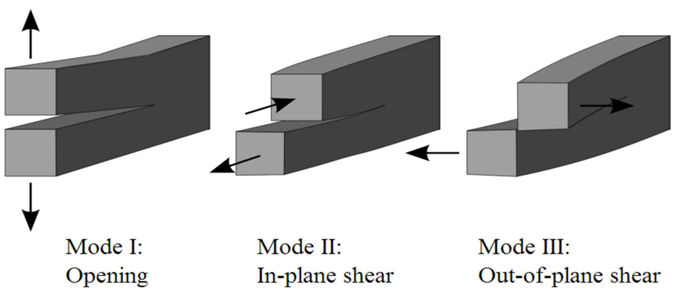

Figure 10 Modes of Fracture

2.6.1 Stress intensity factor

Stress Intensity factor dictates the intensity of stress field in the vicinity of crack. The stress intensity factors are different for the different fracture modes. They are designated as K_I, K_{II} and K_{III} for first, second and third modes of fracture respectively.

$$K = \sigma * Y * \sqrt{(\pi * a)} \qquad \text{Equation 5}$$

Some of the parameters which influence the value of stress intensity factor are :

σ: Applied Stress

Y: also known as geometry factor.

a: Crack depth

2.7 Background Study Of Residual Stresses

Residual stresses are self-equilibrating stresses that would exist in a body if all external loads are removed. Residual stresses will be produced when unevenly distributed non-elastic strains, such as plastic strains, exist. In welding, such plastic strains occur in an area around the weld centreline caused primarily by the dramatic decrease of the material yield stress at very high temperatures. One primary source of residual stresses due to welding is difference in shrinkage of differently heated and cooled areas of welded joint. The weld metal, originally subjected to the highest temperatures, tends upon cooling to contract more than other areas. This contraction is hindered by other parts of the joint, thus resulting in formation of high longitudinal stresses in the weld metal. Similarly, tensile stresses are generated in transverse direction but of comparatively smaller magnitude [18], see Figure 11.

The transition of thermal stress distributions in weld region and HAZ region at various time instants (T_1, T_2, T_3, T_4) during welding has been discussed by Muhammad Siddique as is shown in Figure 11. It is shown that upon cooling process, tensile hoop stress and compressive axial stresses are developed at weld centreline at time instant, T_4, and stress reversal takes place outside this region and maintains force and moment balance in the domain [4].

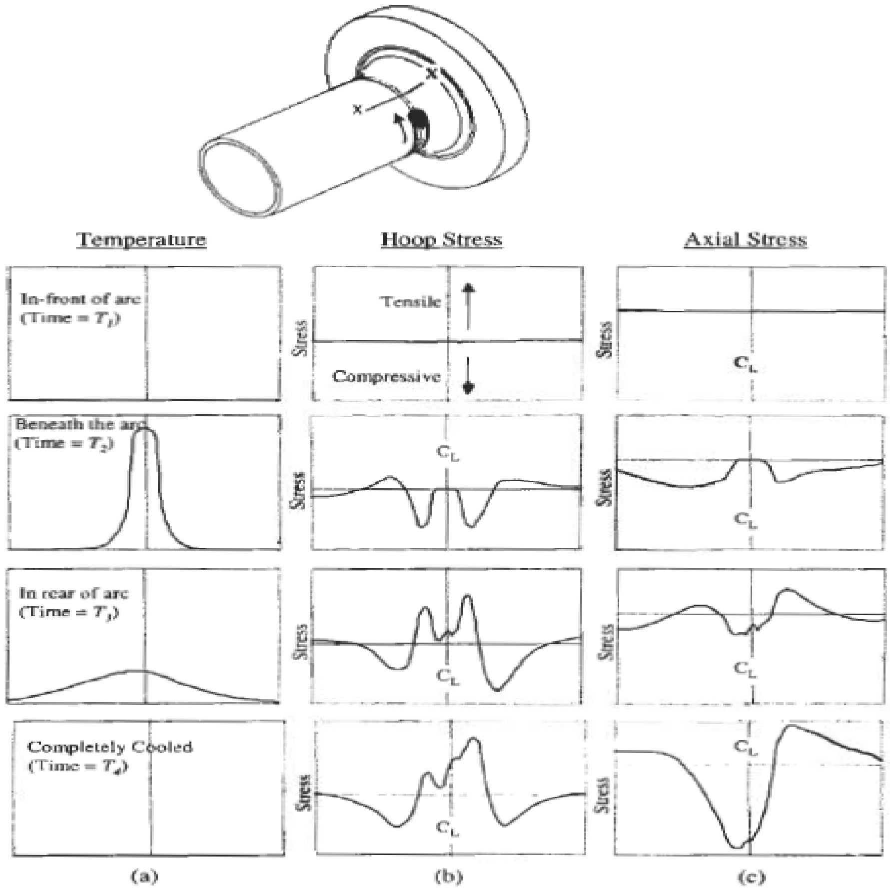

Figure 11 Figure shows the Stress generation and distribution in pipe-flange butt welded joint at various stages of welding(Source : [4]).

In pipes, circumferential butt welds are subject to bending restraint across the weld due to the curvature of the parts being joined [19]. In addition, they are subject to circumferential membrane stresses and axial bending stresses, which are both functions of the radial displacement of the pipe wall [19]. Residual stress distribution in 16 mm x 600 mm API-XL-X65 pipe is discussed by R.H. Leggatt who observed that axial bending stresses increased to peak value at 50 mm from the weld, before decreasing to a negligible value at 175 mm from the weld [19]. These stresses vary along the thickness alternatively from tensile to compressive stresses.

2.7.1 Residual Stress Redistribution During Fatigue Test

Residual stresses can be relaxed by supplying sufficiently high amounts of thermal and/or mechanical energy and thus movement of dislocations which transforms the residual elastic strains to micro plastic strains. This transformation can be done by a combination of dislocation slip, dislocation creep, grain boundary slip and diffusion creep. In other words, relaxation takes place as soon as the summation of load stress (σ_L) and residual stress exceeds material yield strength [20]. The phenomenon of cyclic residual stress relaxation has been observed by Mattson and Coleman [21]. A considerable decrease in compressive residual stresses generated by shot peening on annealed carbon steel under cyclic loading is found by Kodama [22].Residual stress distribution can be seen as a two-step process under cyclic loading : the surface yielding in the first cycle and gradual changes in the following cycles. Residual stresses generated during welding are different from stresses generated by shot peening as welding residual stress is non-uniform in weld zone and heat affected zone. Welding induces some changes in metallurgical behaviour in the weld and its vicinity. Due to these two factors, the residual stress behaviour in welded joints under cyclic loads is complicated [23]. The earliest evidence of detrimental effect of welding residual stress on fatigue appeared in 1956 in reports by Kudryavstev (1956) and Trufyakov (1958) [20]. It was observed that for equal SIF ranges applied , the fatigue crack growth (FCG) rates for as welded joints were higher than FCG rate for base metals. The FCG rates of as welded joints were similar to fatigue crack growth rates of base metals for higher R($\sigma_{min}/\sigma_{max}$) ratios subjected to same SIF ranges [24]. This shows that the entire loading range was contributing to effective SIF range of fatigue damage due to the presence of tensile welding residual stresses and crack was in open state for comparatively longer time per loading cycle. The exact extent of this influence on fatigue strength of material is still under investigation.

Welding residual stresses are considered to have a significant influence on fatigue crack propagation. In cyclic loading, if the summation of load induced stress and welding residual stress exceeds the yield strength of the material, residual stress relaxation takes place [10] as shown in Figure 3. Lopez Martinez(et al) [25] observed stress distributions for as-welded specimens with and without static loading or spectrum fatigue cycling. He concluded that fatigue relaxation in the specimen occurred during the initial cycle of loading and the variable amplitude loading showed the same degree of relaxation as the static load, suggesting that the fatigue relaxation occurred early during the fatigue loading and was correlated to the maximum load in the spectrum as shown in Figure 12.

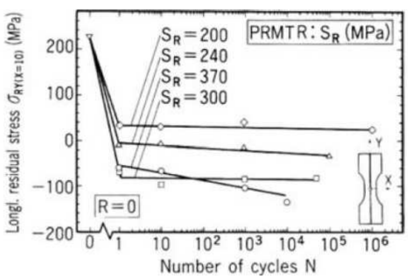

Figure 12 Figure shows change in longitudinal residual stress at a distance 10 mm from weld centre line with application of static fatigue loads [26]

The magnitude of the decrease in the residual stress on the first cycle corresponds with the magnitude of the applied static stress (S_R), indicating a simple shakedown behaviour.

C.D.M Liljedahl [26] carried the tests on MIG welded aluminium plates and applied variable amplitude loading to study the residual stress distribution during the crack growth. He observed initial increase in residual stresses with increasing crack growth and then a gradual decrease in residual stress field with further increase in crack growth. His investigation showed that residual stress distribution is governed by elastic re-distribution and the local crack tip stresses and the associated plastic zone have a minor significance.

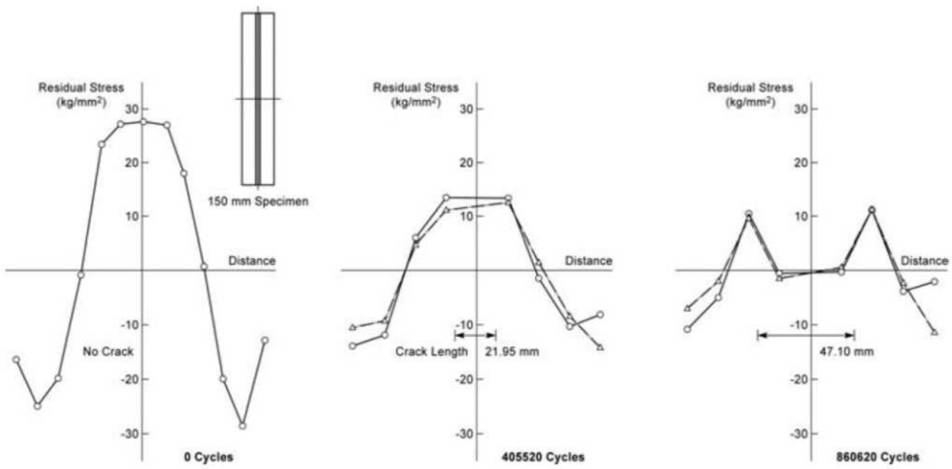

Figure 13 Figure shows transverse distributions of longitudinal residual stresses in smooth butt welded joint before and after fatigue loading [27].

Several researchers [28] [29] [30] have attempted to measure relaxation in residual stress fields resulting from the welding process with fatigue crack extension [31] as shown in Figure 13.The amplitude of the stress cycle applied during fatigue test was small enough that relaxation of the residual stress field due to purely static or cyclic load mechanisms was not significant, as confirmed by measurements before and after substantial fatigue cycling. A continuous decrease in residual stresses is observed with increase in crack growth. Residual stress was assumed to have been elastically relaxed from the initial conditions of stress distribution when the plastic region near the crack tip becomes much smaller than the crack size under the condition of small scale yielding.

2.8 Size Effects

The size of the specimen also influences the fatigue strength. The fatigue strength decreases with increase in size of specimen. The total strength of component may increase, but the allowable stress decreases. This is known as size effect and is caused by [13]:

A statistical defect. When the size of a component increases, the chance of a 'weak link', in the form of small inclusion or residual stress, increases. Therefore, the chance of an initiating crack increases.

A technological size effect. The production processes and their associated surface conditions upon delivery have an influence on the fatigue strength of a component.

A geometrical size effect. When the thickness of a plate increases the stress gradient at a notch decreases. When the inclusions or surface defects have the same size as they have in thinner plate, the zone of tensile stresses at the tip of a defect are larger in the case of a thick plate.

A stress increase effect. When the plate thickness increases, the notch size in general does not scale up to same amount, or may not scale at all. The ratio between the notch radius and plate thickness becomes smaller for thicker plates so that the notch stress is increased.

Codes [3] allow the use of fatigue data of plate strip specimens to relate to full scale pipe specimens. However, there is always a possibility that fatigue data obtained from testing of plate strips specimens is different from actual fatigue behaviour of full scale pipes. It may be due to the fact that with increase in volume of material increases the probability of presence of defects in the pipe specimens. The manufacturing process for plate strip specimens is also different from manufacturing process of pipes which lead to difference in surface properties in these specimens. The residual stresses produced during different fabrication processes will be different for these specimens.

A better way to assess the fatigue life of pipe specimens would be to extract the strip specimens from the full scale pipes. The fatigue data is collected from strip specimens cut from the line pipe. It will provide better estimate as this will contain almost all stresses and flaws in the material generated during fabrication of pipe and will reflect the behaviour of pipe under similar loading conditions. These stresses can be residual stresses generated during the fabrication process. It is argued that residual stresses are relieved when the strip specimen is cut from the full scale pipe [32]. The uncertainties due to size effect should be considered when comparing the strip specimen fatigue test data with full scale pipe test data.

2.9 Objective

During literature review, it is found that it is critical to study the crack propagation rate in strip specimen and pipe specimen under similar conditions. There is also a need to investigate the influence of residual stresses exclusively on crack propagation rate. This thesis study is carried out with following objectives:

- to investigate the influence of residual stresses on fatigue crack growth rate in pipe specimens.

- to investigate and compare crack growth rate of strip specimen and line pipe using experimental results.

These objectives are met by performing full scale four point bend fatigue tests on pipes with different conditions and three point single edge notch bend fatigue (3 SENB) tests on strip specimens extracted from the same pipes.

3 EXPERIMENTAL SET-UP AND METHODOLOGY

In this chapter, the design of test-rig and measurement systems used for carrying out fatigue tests are discussed. In section 3.1 and 3.2, the design of the test-rig is explained. In Section 3.3, the approach used for crack growth monitoring is discussed. In Section 3.4, specimens geometry and material properties are explained. Section 3.5 discusses the accuracy of systems used during fatigue tests.

3.1 Test Rig

In this research study, four point bend fatigue tests are performed on 114.3 mm diameter pipes to study the influence of residual stresses on fatigue crack growth rate in pipe specimens. A test-rig is designed and constructed for carrying out four point bend fatigue tests using a combination of HEB-200 I-Beams and saddles. It is found during analytical calculations that stiffness of pipe specimen is considerable, so HEB-200 I-Beam having higher stiffness compared to pipe specimen is selected after analytical and numerical calculations. As the load levels applied (300 KN-150 KN) are high, the I-Beam is checked for strength, stiffness and stability using NEN-6770:1997 code [Appendix-A]. Stiffeners are used on upper I-Beam to prevent lateral buckling as discussed in Section 3.2. The four point bending test rig is shown in Figure 14 and the schematic diagram of the assembly is shown in Figure 15.

Figure 14 Pipe specimen with surface notch loaded in four point bend test-rig.

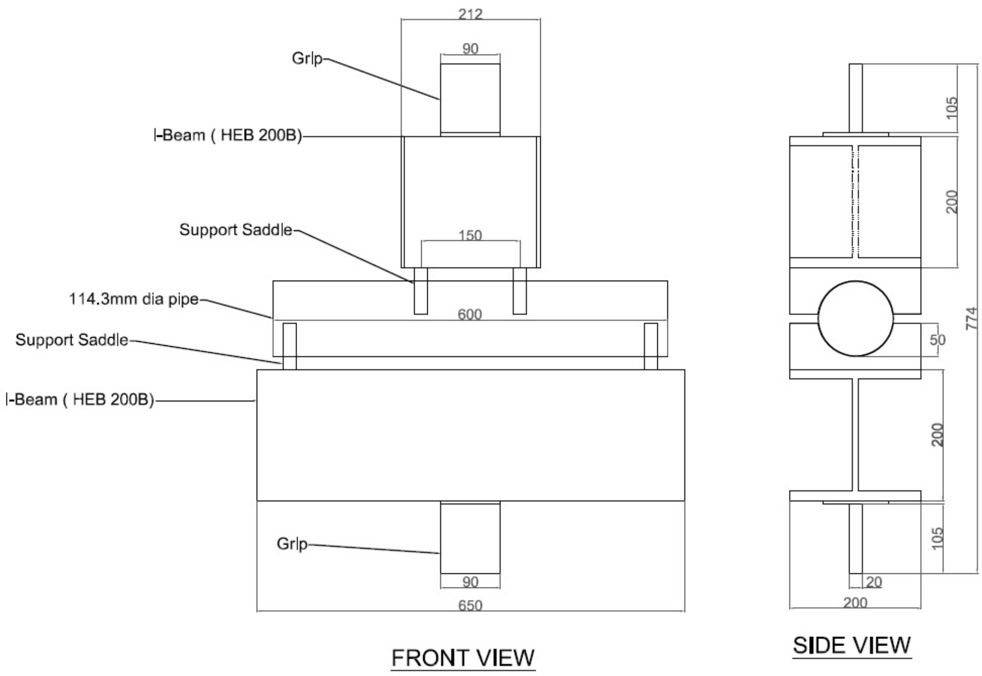

Figure 15 Schematic diagram of test rig used for fatigue tests.

Local buckling of pipe specimen was expected at point contacts because of large loads. Therefore, semi-circular saddles are designed to apply loads over a surface area. Another advantage of such shape is that the semi-circular shape will restrain the pipe specimen from bulging outwards at the ends. The thickness of saddles are 20 mm. The radius of curvature of saddle is decided as 58 mm to accommodate insulation strip between the pipe specimen and the saddles. Electric Discharge Machining is used to create a semi-circular profile on saddles with $\pm$0.1 mm accuracy. The geometrical details of saddle is shown in Figure 16.

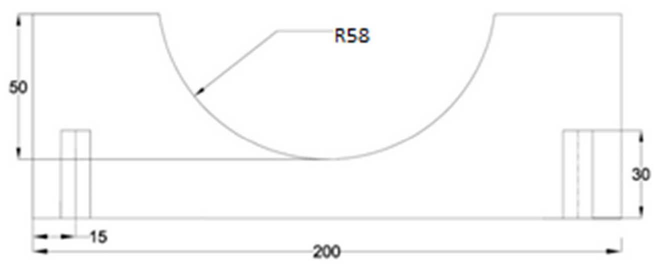

Figure 16 Schematic diagram of Saddle

The saddles and pipe are checked for plastic yielding using Finite element analysis (FEM) in Abaqus. During FEM analysis, the maximum stresses generated in saddle at contact area is found to be 540 MPa as shown in Figure 17, so the material of construction for saddles is chosen as S690 (Yield strength = 690 MPa).

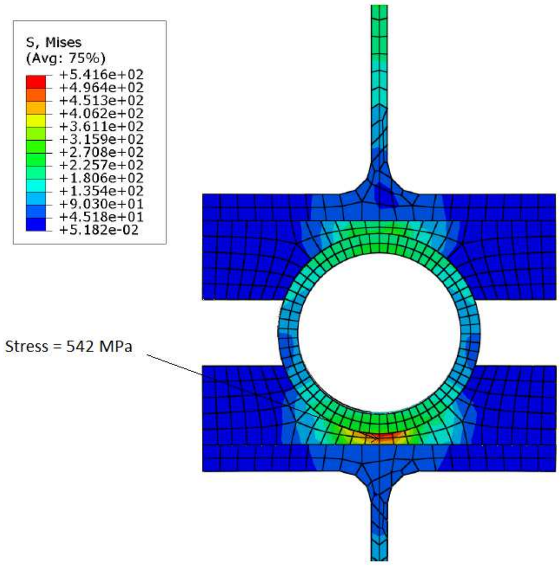

Figure 17 Figure shows FEM simulation depicting maximum stress generated in contact area at maximum load condition.

3.2 Sensitivity Analysis Of Test Rig

The design of test-rig is checked for stability against any inherent misalignment in MTS machine or misalignment in the test rig set-up at design load conditions. It is done by analysing the influence of shift in the load application point in the transverse direction at top and bottom lips of the test-rig using FEM. Lateral bending of the beam is observed during the FEM analysis for a transverse displacement of 10 mm of load application point. The use of stiffeners is recommended after finite element analysis to avoid lateral beam buckling for this situation during the test. A misalignment of 5 mm is found between the upper and lower head of MTS machine during the test conditions. The stiffeners prevented the I Beam from buckling but lateral bending of plate attached to beam is observed during the start of fatigue test. A thin plate of 5 mm is inserted between the grips and lip to tackle this problem so that the upper and lower half of the test-rig aligns during the test. The alignment of the test-rig is checked visually before and during fatigue tests.

3.3 Crack Growth Measurement

3.3.1 Direct Current Potential Drop (DCPD)

In this research study, it is required to monitor the crack depths continuously to study the crack propagation rate. Various methods were considered to monitor the crack propagation during literature survey as discussed in Section 2.5. Direct current potential drop method is considered suitable for crack growth measurement for the fatigue tests in combination with method of beachmarks and optical measurements. In direct current potential drop method, a direct current is caused to flow in pipe specimen and the voltage drop developed across the crack is measured. This voltage drop is a function of the electrical properties of specimen material and geometry of the specimen and of crack length. The direct current potential drop set-up used in these tests consists of Pulsed Direct Current Potentiometer (Howden), current electrodes and potential probes. X- and Y- electrical probes are attached to the pipe specimen by spot welding near the notch region for measuring the change in potential drop values as shown in Figure 18.

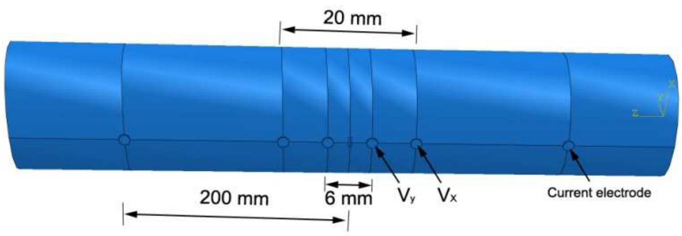

Figure 18 Figure shows the potential drop probes and current electrode connections in the pipe specimen.

For pipe specimens, the gains of both the X and Y probes are adjusted to increase the sensitivity of potential drop to detect crack propagation and decrease the noise level. Since the size of the pipe specimen is large, a gain of 5 is applied at the near probes (V_y) and a gain of 1 is applied at outer probes (V_x).

$$V_r = V_x/V_y \qquad \text{Equation 6}$$

This method is chosen to reduce the noise in the output signal and increase the sensitivity of the DCPD method. The pipe specimen is electrically insulated from the test-rig by using glass fibres strips placed between pipe specimens and saddles. The pipe specimens are checked for electrical isolation using voltmeter.

In Strip specimens, M- and N- electrical probes are fixed to the strip specimen by spot welding at 3 mm and 30 mm distance on either side of notch for measuring the change in potential drop values as shown in Figure 19. Two holes of M4 are drilled at both ends of specimens for connecting current electrodes of Pulsed DC potentiometer used to study crack propagation.

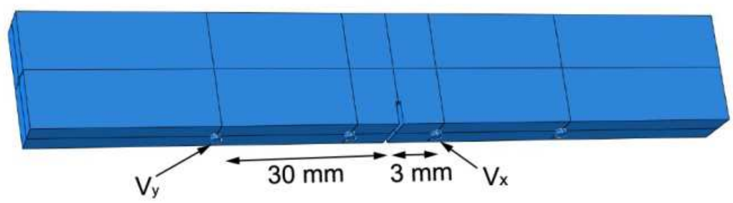

Figure 19 Figure shows the distance of potential drop probe position from notch centre in strip specimen.

The gains of both the X and Y probes are adjusted to increase the sensitivity of potential drop to crack propagation and decrease the noise level. A gain of 0.5 is applied at the near probes (V_y) and a gain of 1 is applied at outer probes (V_x). The Potential drop values are calculated using following relation.

$$V_r = V_x/V_y \quad \text{Equation 7}$$

3.3.2 Method Of Beachmarks

For shallow surface crack in non-transparent materials, it is not possible to monitor crack depth propagation through optical measurements. So, direct current potential drop (DCPD) method and method of beachmarks are used in combination to monitor the crack growth along depth direction efficiently. In beachmarks method, parallel stripes are created at regular intervals of 1 mm (approximately) on both sides of surface notch in circumferential direction by using Calliper. Beachmarks are produced during fatigue tests due to change in crack growth conditions, such as a change in environment or stress level or a pause in stress cycling (interruption in service) [33]. In this research, Variable amplitude fatigue test is performed to produce beachmarks by varying stress levels applied. In this test, load ratio is changed to next load block for a particular increase in circumferential crack length. Minimum load applied is varied among all load blocks keeping the maximum load value constant. Visible beachmarks are produced corresponding to each load block as shown in Figure 20.

Figure 20 Figure shows the initial semi-elliptical notch and beachmarks produced during variable amplitude fatigue test in cracked region in pipe specimen.

The pipe specimen is broken at the crack location and images are taken using stereo microscope to relate the surface crack length 'c' with crack depth 'a'. A relation is then developed relating crack depths as a function of surface crack lengths. All pipe specimens are broken after the test to confirm that the aspect ratio(a/c) of the crack front is approximately same for all fatigue tests.

3.3.3 DCPD data processing for crack growth rate calculation

The data obtained from DCPD measurements is used to calculate crack size during the fatigue test in combination with visual measurements. However, there is inherent noise in potential drop data which is uniform throughout the test. The noise in the potential drop data is of the order of 20 mV/cycle and the potential drop for a unit increase in crack length is observed as 30 mV during fatigue test. The potential drop for an unit increase is small because there was a smaller current density in notch region due to large geometry of specimen.

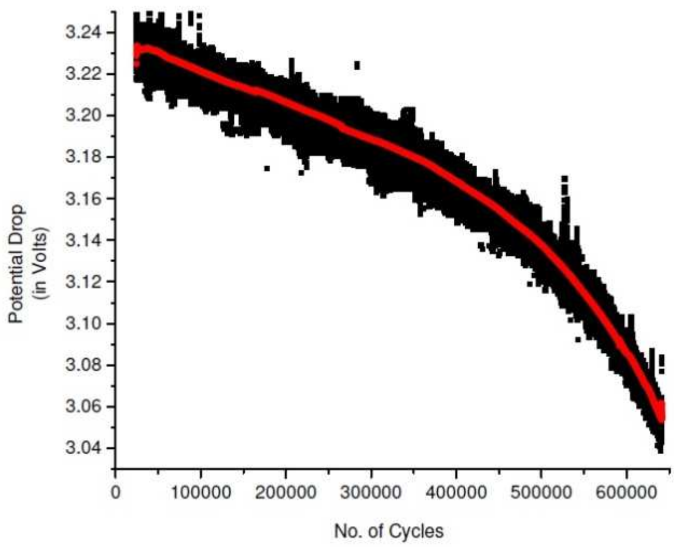

Figure 21 Figure shows raw DCPD data and smoothened curve using adjacent averaging method.

Therefore, DCPD data need to be processed to reduce this noise for calculation of crack growth rate. The methodology used for data processing is mainly governed by the magnitude of noise in DCPD data and the number of cycles taken for a characteristics crack growth. The noise is reduced by smoothing the data using adjacent averaging method. In this method, the values are averaged over a moving interval of cycles needed to measure detectable crack size change(Δa) during experiment as shown in Figure 21.The width of the interval is varied in steps to analyse the effect of interval width on the reliability of crack growth calculation.

The width of the interval chosen is such that it reduces the noise without affecting the reliability of DCPD data. It is seen that increasing the width of interval helps in smoothing the data without decreasing the reliability till interval width of 10^5 as shown in Figure 22.

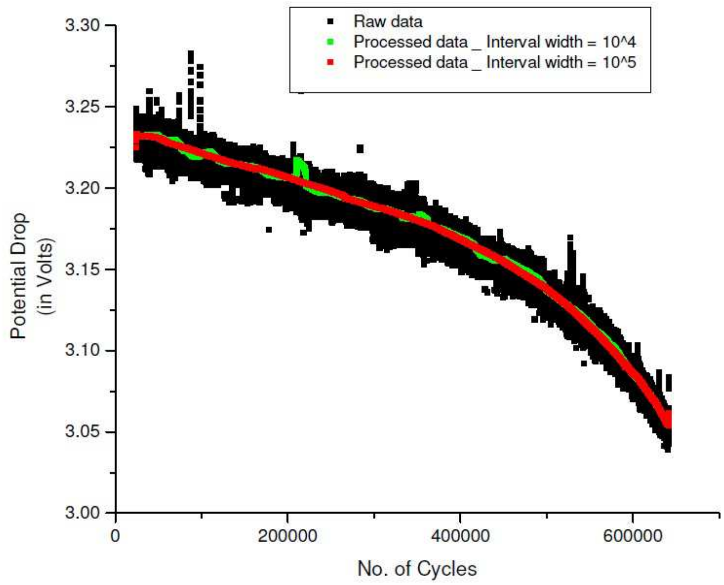

Figure 22 Figure shows the influence of moving interval width selected on the width of smoothened DCPD data using adjacent averaging method.

It might be because the number of cycles for 1mm increase is of the order of 10^5 for most portion of fatigue test. However, the number of cycles for 1mm crack growth is of the order 10^4 for last 50000 cycles. So, the width of interval for DCPD data corresponding to that portion of fatigue test is kept as 5000 points. The DCPD data is then calibrated by using optical measurements noted for crack lengths 'c' during fatigue test. A calibration curve is then generated for relating crack size measurements with potential drop values for all tests. The crack size is then calculated by using DCPD data and compared with optical readings taken during the test as shown in Figure 23. The crack growth rate is then calculated from these crack size values by differentiating crack size with respect to number of cycles , i.e., da/dN.

The treatment of DCPD data for strip specimens is done by using similar method. The width of interval in adjacent averaging method chosen is comparatively small because the potential drop for characteristic crack growth was significantly larger than the noise in DCPD data.

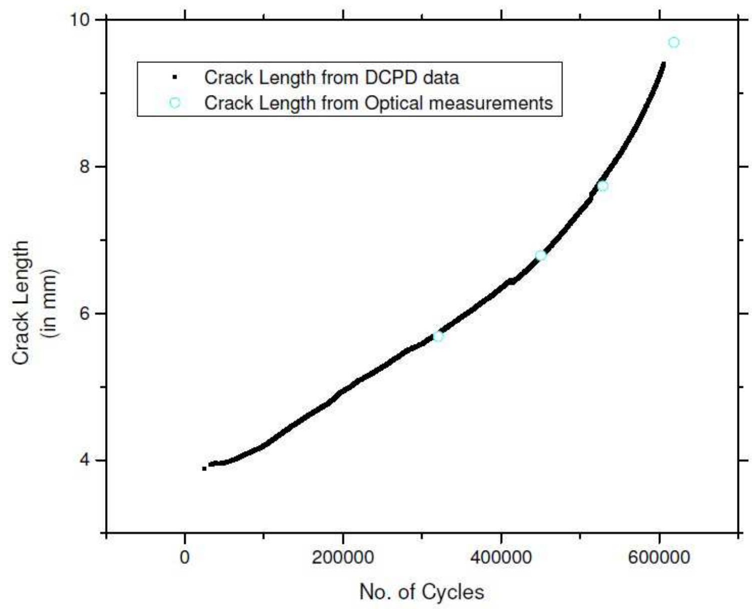

Figure 23 Figure shows the comparison of calculated crack lengths(c) by using DCPD data and optical measurements taken during test.

3.4 Specimen Geometry And Material Specification

3.4.1 Pipe Specimen

In fatigue tests, scatter is commonly observed in experimental data. Microstructure change and surface quality change among specimens are common sources of such scatter. To reduce the effects of such sources, six pipe specimens of equal length were extracted from a single pipe of 12 m length. The material properties and dimensions are taken from pipe data sheet as shown in Appendix-B. The diameter of pipe specimen is 114.3 mm and thickness is 11.1 mm [Appendix-B]. The average length of pipe specimen cut from the pipe is 725 mm. The loading points and support point locations is decided based on analytical calculation[Appendix-C] and FEM analysis and are shown in Figure 24. The yield strength of pipe material is 541 MPa and the tensile strength is 595 MPa [Appendix-B]. Two holes of M4 are drilled on both sides of notch for connecting current electrodes of Pulsed DC potentiometer. The distance of the holes from the edge of notch is kept as 200 mm to ensure uniform current density in the notch region. There is always an uncertainty about the crack initiation site in fatigue test. To minimise this uncertainty and facilitate crack initiation, a semi-elliptical notch is created in middle of specimen length using LASER machining process as explained in Section 3.4.3. The pipe surface near notch region is cleaned by wire brush before notch machining to remove any rust and polished after notch machining until 2400 grit.

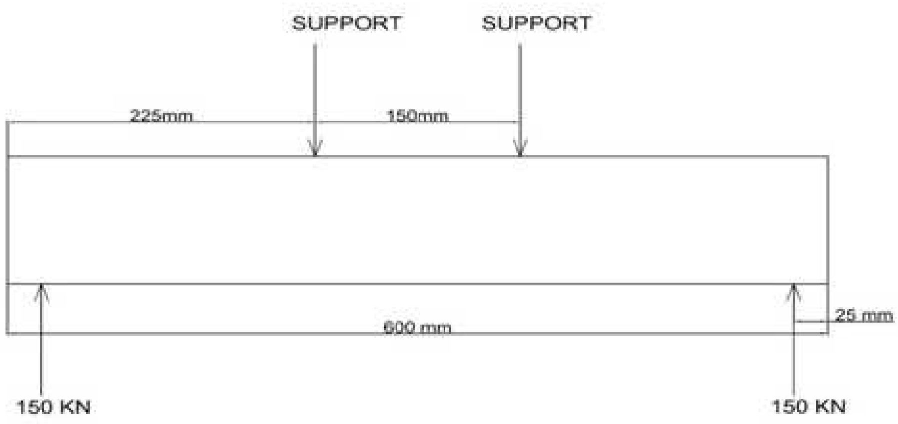

Figure 24 Figure shows dimensions of pipe specimen and the positions of forces applied & support locations.

3.4.2 Pipe Specimens with residual stresses

Pipe specimen is cleaned by removing rust in notch region by using wire brush and sand paper until 2400 grit. Fusion welding process is used for generation of residual stresses in the pipe wall at notch region. The weld passes are applied at 23 mm distance from notch centreline on both sides of notch. The pipe specimens are treated by Tungsten Inert Gas (TIG) arc under controlled conditions to generate residual stresses along pipe wall thickness. Since the stress generated at notch region is due to bending strains developed at fusion welded zone, a linearly varying stress gradient is generated along wall thickness as discussed in Section 5.1 [Appendix-D]. The test-set up for thermal treatment is shown in Figure 25. The pipe specimen is rotated at required constant speed of 2 mm/sec using rotating machine decided by the FEM simulation discussed in Section 5.1. The input current applied is 150 A and the distance between the welding torch and pipe surface is maintained at 4 mm$\pm$1 mm. The start and end point of welding process is at points on the opposite sides of the notch as the arc is not stabilised at the start of the welding process.

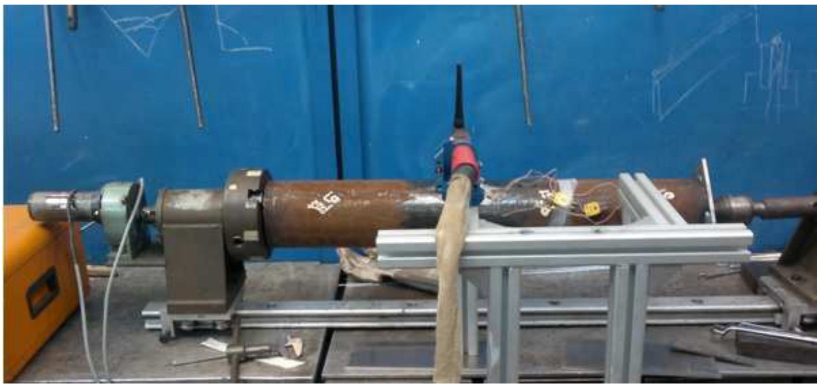

Figure 25 Figure shows test set up used for fusion welding in the vicinity of notch region using Metal Inert Gas welding machine (MIG).

3.4.3 Strip Specimen

Two strips are extracted from pipes for three point bend fatigue tests. The curved surface on both sides are machined using milling machine to create rectangular specimen. The dimensions and material of both specimens are shown in Table 1.

S. No	Specimen	Material	Thickness (in mm)	Width (in mm)
1	Specimen-1	API X-65	9mm	25.5
2	Specimen-2	API X-65	7mm	30

Table 1 Dimension and properties of Strip Specimen

The geometry of the strip specimens are decided in accordance with ISO 12108. The thickness of the specimen should be in range 0.2W - W [34] where W is the width of the specimen. Two holes of M4 were drilled on both sides of specimen for connecting current electrodes. The geometrical details of specimen-1 and specimen-2 are shown in Figure 26 and Figure 27.

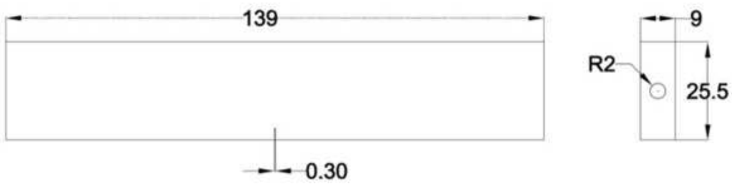

Figure 26 Figure shows geometrical details of Specimen-1. (All dimensions are in mm)

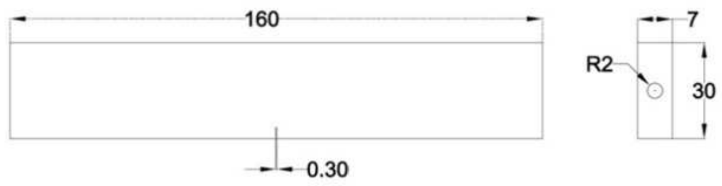

Figure 27 Figure shows geometrical details of Specimen-2. (All dimensions are in mm)

3.4.4 Notch machining on pipe specimen

A semi-elliptical circumferential notch is machined on external surface of every pipe specimen in the centre by LASER (Light amplification by stimulated emission of radiation) to decrease the crack initiation phase and facilitate crack initiation at preferential location during the fatigue tests. The length (2c) of the notch is 8 mm and the depth of notch (a) is 1 mm. The width of the notch at the top surface is 1 mm and the bottom tip of the notch is kept as 0.1mm wide to increase the stress concentration in that region. The shape of the notch generated in pipe specimen is shown in Figure 28 and Figure 29.

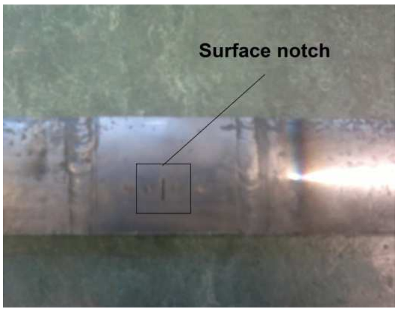

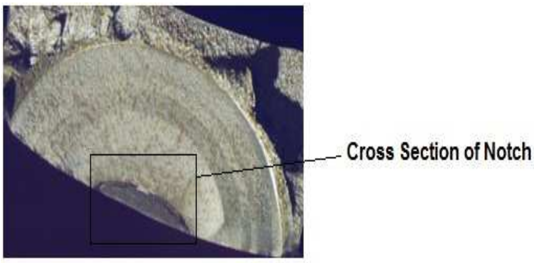

Figure 28 Figure shows surface notch on pipe specimen and cross section of notch in cracked region.

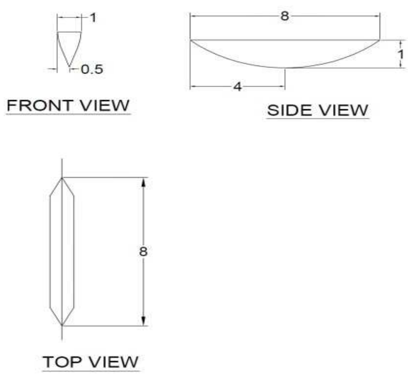

Figure 29 Figure shows geometrical details of semi-elliptical notch machined on pipe specimen using LASER.

3.4.5 Notch machining on strip specimens

A through thickness notch is machined in strip specimen by using diamond saw disc of 0.3 mm thickness. The notch is machined at the centre of specimen with a tolerance of $\pm 0.005W$. For specimen-1, the notch length (c) is 2.5 mm and the height of notch is 0.3 mm [34] as shown in Figure 30. The notch length for specimen-2 is kept as 3 mm and notch height (h) as 0.3 mm as shown in Figure 31.

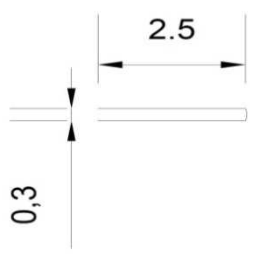

Figure 30 Notch dimensions for Specimen-1

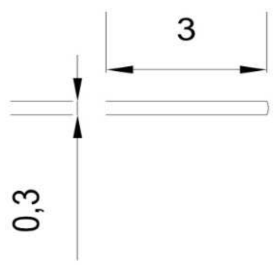

Figure 31 Notch Dimensions for Specimen-2

3.5 Accuracy Of Measurement Systems

In this section, the potential sources of introduction of errors and uncertainties associated with the experiment are discussed.

3.5.1 Specimen geometry

The six pipe specimens are extracted from one pipe of 12 m length. The length of each pipe specimen is 700-720 mm in length. The pipe length between outer supports is not important for bending moment generation in the notch region. The variation in pipe span outside the load points does not contribute to errors in experiment.

3.5.2 Error in Crack Size Measurement

Optical measurements are taken after specific number of cycles to measure surface crack length. An error of ± 0.2 mm is considered in these measurements. These errors are random and can be reduced by repeating the experiments.

3.5.3 Fatigue testing machine

All fatigue testing machines control loads applied by the measurements from load sensor in load cell located at the top of machine. The load sensor measures load with an accuracy of 0.001%. The accuracy of load sensor measurements is thus ±350 N.

3.5.4 Potential Drop Measurement

The potential drop data is prone to errors due to changes in geometry, input current. So, a calibration curve for every test specimen is prepared to relate the potential drop values with surface crack length to minimize this error. The error due to changes in temperature, material resistivity are considered small and neglected.

4 PIPE SPECIMEN WITHOUT RESIDUAL STRESS

In this chapter, the experimental procedure and results for the variable amplitude and constant amplitude fatigue tests are discussed. In Section 4.1, procedure and results of variable amplitude fatigue test performed to generate the beachmarks on pipe cross sectional area are discussed. The details of constant amplitude fatigue tests on pipe specimens are discussed in Section 4.2.

4.1 Variable Amplitude Fatigue Test

One of the objectives of this research study is to study the influence of residual stress on crack growth rate along the pipe wall thickness. It is required to measure the crack depth positions at specific cycle intervals to calculate the crack growth rate during fatigue test. During literature review, it is found that it is difficult to measure the crack depth positions by non-destructive tests alone during fatigue test. A variable amplitude fatigue test is selected and performed to produce beachmarks to measure the crack depth [15] [16]. In this test, various load blocks of different stress ratios are applied for specific number of cycles during the test as discussed in Section 3.3.2. The minimum load applied is varied among load blocks keeping the maximum load constant. The various load blocks applied during the test are shown in Table-2.

The Beachmarks generated are used to investigate the crack front shape and to generate a relation between crack length and crack depth during crack propagation at different cycle intervals during fatigue test. Three load blocks of different stress ratios are applied during the variable amplitude fatigue test for the generation of beachmarks.

Block No.	Number of Cycles	Stress Ratio	Max. Stress (in MPa)	Min. Stress (in MPa)
1	0 - 89176	0.1	335	35
2	89176 - 166758	0.5	335	162
3	166758 - 263976	0.8	335	268
4	263976 - 268520	0.1	335	35
5	268520 - 307092	0.5	335	162

Table 2 Details of Load Blocks applied during fatigue test to produce beachmarks.

This research study intends to investigate the crack growth stage so a semi-elliptical notch is created on each pipe specimen to decrease the crack initiation phase and to facilitate the crack initiation at preferred position during fatigue test. The depth(a) of notch is 1 mm and the length (2c) is 8 mm. The notch dimensions are decided by considering uniform stress values at notch depth and notch tip on crack perimeter calculated by FEM analysis.

Surface crack lengths at the start and end of each load block are measured by optical measurements. A strip specimen containing the cracked region is cut from the pipe specimen after the test and is broken at the region of beachmarks. Due to the change in stress ratio during the various load blocks, beachmarks are produced on the pipe cross section as shown in Figure 32. The crack depth is measured by Stereo microscope corresponding to surface crack lengths.

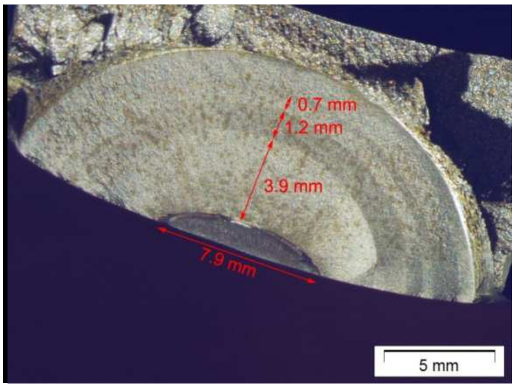

Figure 32 Figure shows crack depth positions measured by using beachmarks produced in variable amplitude fatigue test.

The crack growth data collected from variable amplitude test is used to generate a relation curve between surface crack lengths and crack depths as shown in Figure 33. This curve is used to calculate crack depth and crack sizes in subsequent pipe tests.

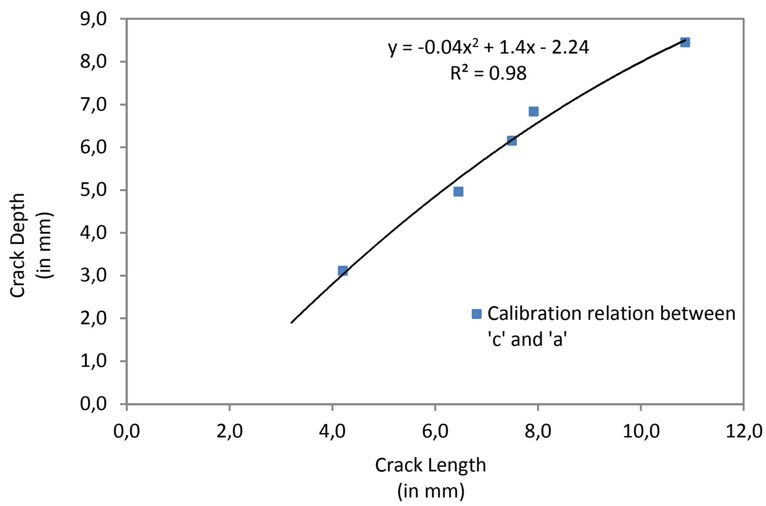

Figure 33 Figure shows calibration curve between crack length(c) and crack depth(a).

4.2 Constant Amplitude Fatigue Test

Two pipe specimens are tested under constant amplitude cyclic loads to investigate the crack growth behaviour in notched pipe specimen without residual stresses. The pipe specimens are loaded with constant stress range of 163 MPa during the crack growth stage. The stresses applied are 335 MPa(maximum) & 162 MPa(minimum) and the stress ratio($\sigma_{min}/\sigma_{max}$) is 0.5. The frequency of cyclic loading used is 3 Hz and the environment is lab air of room temperature. The time duration for one fatigue test is seven days.

A semi-elliptical notch is machined using LASER process to create weak link in the centre of pipe specimens to avoid crack initiation at undesired locations. A weak link is the point where the stress concentration is highest which could be due to the presence of rough geometry, residual stresses or notch. The notch length(2c) on surface is 8 mm and the depth(a) of the notch is 1 mm as shown in Figure 28 and Figure 29. The notch is created in a way that sharp corners are developed at the edges to generate high stress concentration during fatigue test. Semi-elliptical shape is chosen for the machined notch as crack usually has a tendency to grow in semi-elliptical shape [35] [36]. The experimental readings of crack length, c, and the corresponding number of cycles, N, are recorded periodically after suitable crack increments. Pulsed DC potential drop monitor(Howden) is used to collect potential drop data during fatigue tests.

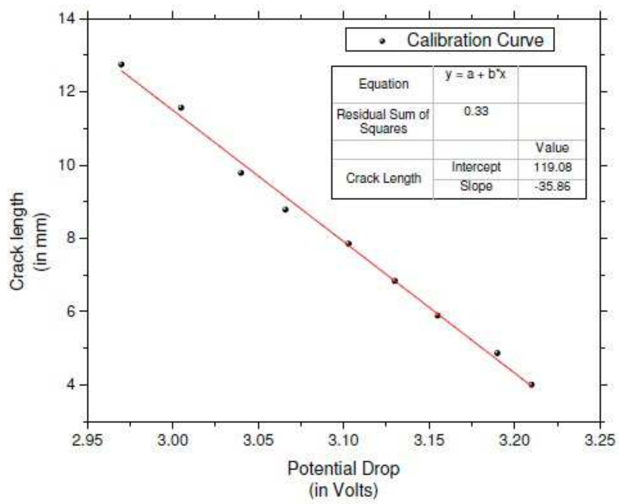

Figure 34 Figure shows calibration curve between crack length(c) and potential drop prepared by using optical measurements.

The potential drop readings from potential drop monitor and optical measurements of surface crack length are noted regularly during fatigue test. The crack length values and potential drop values are then used to create a calibration curve for continuous variation of surface crack lengths as a function of potential drop values as shown in Figure 34. The values of surface crack lengths are then used for calculating crack depth values as discussed in Section 4.1.

The potential drop data obtained from Howden machine is processed to minimise the scatter as discussed and calibrated with respect to optical measurements to calculate crack length(c) values as discussed in Section 3.3.3. The processed data is then used to generate da/dN curve as a function of stress intensity factor range(ΔK). The stress intensity factor range(ΔK_I) for surface flaws is calculated using Equation 8 as per BS7910 [3] [37].

$$\Delta K_I = Y.(\Delta\sigma)\sqrt{(\pi a)} \qquad \text{Equation 8}$$

where (Y.Δσ) considers overall contributions from primary and secondary stresses and 'a' represents crack length at which stress intensity factor range has to be calculated. (Y.Δσ) is calculated by using Equation 9.

$$(Y.\Delta\sigma)_p = Mf_w[k_{tm}M_{km}M_m\Delta\sigma_m + k_{tb}M_{kb}M_b\{\Delta\sigma_b + (k_m - 1)\Delta\sigma_m\}] \qquad \text{Equation 9}$$

For surface flaws in plates and pipes, M=1, k_{tm}=1, M_{km}=1, k_{tb} = 1, M_{kb} = 1 are considered for calculation of $(Y.\Delta\sigma)_p$ according to BS7910 [3]. $\Delta\sigma_m$ and $\Delta\sigma_b$ are membrane and bending stress ranges applied. If the actual flaw area is greater than 10% of the load bearing cross section area (generally B.W), K_I should be multiplied by the f_w factor. The value of f_w is calculated by Equation 10.

$$f_w = \{sec[(\pi c/W)(a/B)^{0.5}]\}^{0.5} \qquad \text{Equation 10}$$

Here, width, W = (2*π*r) = 358.9 mm

and thickness, B =11.1 mm

The value of M_m is calculated by using Equation 11 given in section M.3.2.2.2 of BS 7910 [3].

$$M_m = \{M_1 + M_2(a/B)^2 + M_3(a/B)^4\}gf_\theta/\varphi \qquad \text{Equation 11}$$

and M_1, M_2, M_3, g, f_θ and ϕ are calculated using following equations applicable for given aspect ratios as per BS 7910.

$$M_1 = 1.13 - 0.09(a/c) \qquad \text{for } 0 < a/2c \leq 1 \qquad \text{Equation 12}$$

$$M_2 = [0.89/\{0.2 + (a/c)\}] - 0.54 \qquad \text{for } 0 \leq a/2c \leq 0.5 \qquad \text{Equation 13}$$

$$M_3 = 0.5 - 1/\{0.65 + (a/c)\} + 14\{1 - (a/c)\}^{24} \quad \text{for } a/2c \leq 0.5 \quad \text{Equation 14}$$

$$g = 1 + \{0.1 + 0.35(a/B)^2\}(1 - sin\theta)^2 \quad \text{for } a/2c \leq 0.5 \quad \text{Equation 15}$$

$$f_\theta = \{(a/c)^2 cos^2\theta + sin^2\theta\}^{0.25} \quad \text{for } 0 \leq a/2c \leq 0.5 \quad \text{Equation 16}$$

$$\varphi = \{1 + 1.464(a/c)^{1.65}\}^{0.5} \quad \text{for } 0 \leq a/2c \leq 0.5 \quad \text{Equation 17}$$

M_b is calculated by using following expression.

$$M_b = H * M_m \quad \text{Equation 18}$$

where M_m is calculated from Equation 11 and 'H' is calculated by using following equations.

$$H = H1 + (H2 - H1)sin^q\theta \quad \text{Equation 19}$$

$$H_1 = 1 - 0.34(a/B) - 0.11(a/c)(a/B) \quad \text{for } 0 \leq a/2c \leq 0.5 \quad \text{Equation 20}$$

$$H_2 = 1 + G_1(a/B) + G_2(a/B)^2 \quad \text{Equation 21}$$

$$G_1 = -1.22 - 0.12(a/c) \quad \text{for } 0 \leq a/2c \leq 0.5 \quad \text{Equation 22}$$

$$G_2 = 0.55 - 1.05(a/c)^{0.75} + 0.47(a/c)^{1.5} \quad \text{for } 0 \leq a/2c \leq 0.5 \quad \text{Equation 23}$$

The data collected from the experiments is processed and plotted in suitable scales to analyse the crack propagation behaviour during different stages of fatigue test. The surface crack length(c) growth is plotted with respect to number of cycles on a log-log scale to observe the crack growth rate during fatigue test as shown in Figure 35. It is seen that there is difference in crack length magnitudes in Test-1 and Test-2. It could be attributed to the variation in number of load cycles of specific load range which were applied during crack initiation phase. In all fatigue tests, load range of 270 KN is applied to decrease the crack initiation period. In Test-1, the number of cycles applied were 32000. But, it was observed that application of high load range led to frequent damage of insulating material used during fatigue test. Therefore, it was decided to decrease the number of cycles of 270 KN load range to 24,000 cycles in the subsequent tests. This might be the reason for larger crack length in Test-1 as compared to Test-2 for a specific cycle number. However, it does not influence the slope of crack growth during later portion of fatigue test. The data is thus used to compare with crack growth curves of second test condition as discussed in Section 7.4.

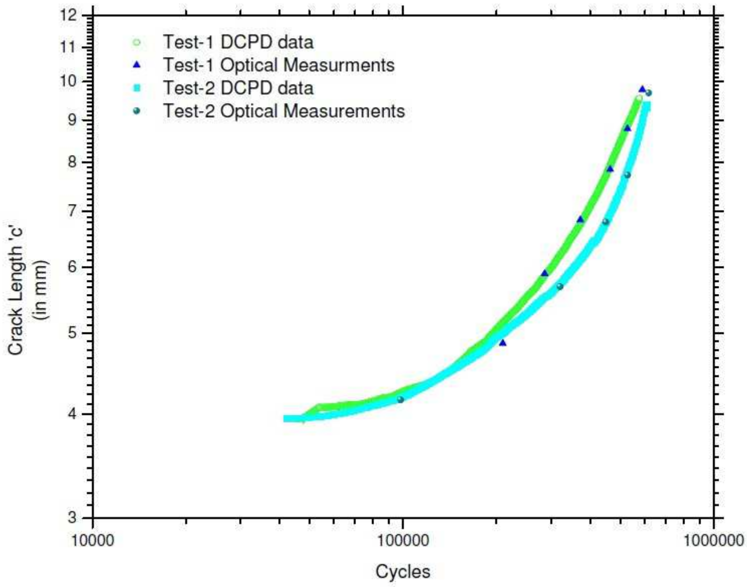

Figure 35 Figure shows crack Length(c) propagation with respect to number of cycles for pipe specimens without residual stresses.

It is observed during variable amplitude fatigue test that crack front grows non-uniformly in all directions during initial portion of fatigue test. The crack depth growth is plotted with respect to number of cycles to study crack depth growth rate during fatigue test as shown in Figure 36.

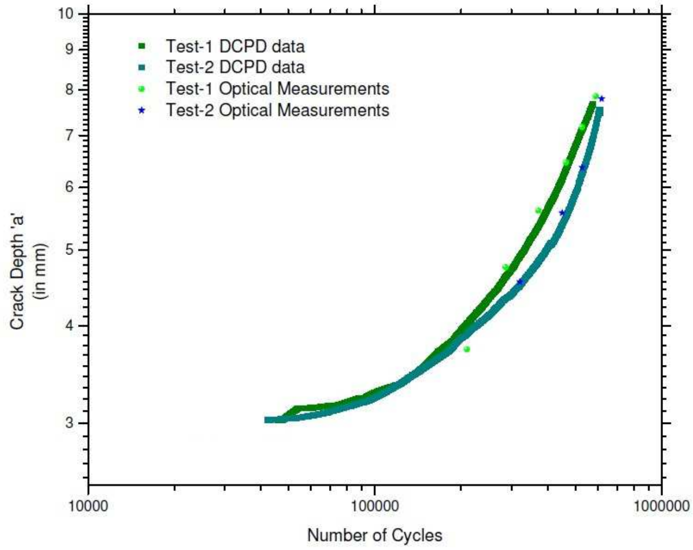

Figure 36 Figure shows crack depth (a) propagation with respect to number of cycles for pipe specimens without residual stress.

The crack length growth rate (dc/dN) is plotted with respect to SIF range (ΔK_c) on a log-log scale to study the crack length growth behaviour with stress intensity factor ranges as shown in Figure 37.

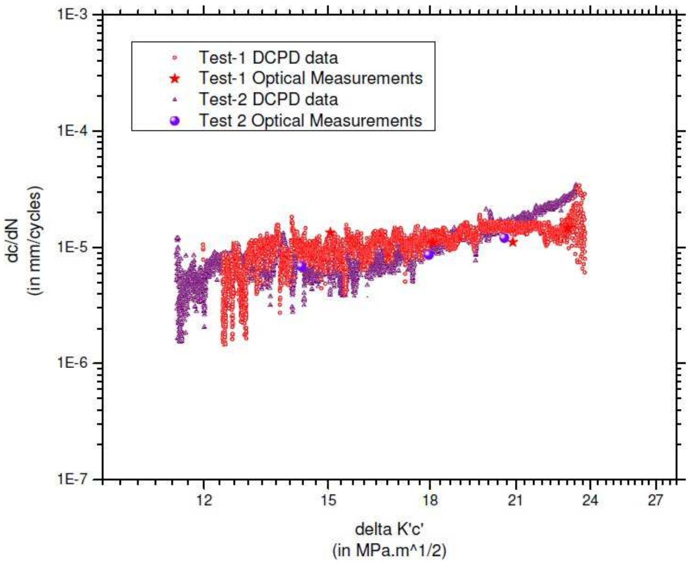

Figure 37 Figure shows comparison of the crack length growth rates (dc/dN) between pipe specimens without residual stress.

Optical measurements are also added in the graph along with DCPD data to compare the accuracy and reliability of DCPD data. The graph shows that DCPD data is in good agreement with optical measurements.

Similarly, the crack depth growth rate (da/dN) is plotted with respect to SIF range (ΔK_a) to study the crack depth growth behaviour with stress intensity factor ranges as shown in Figure 38.

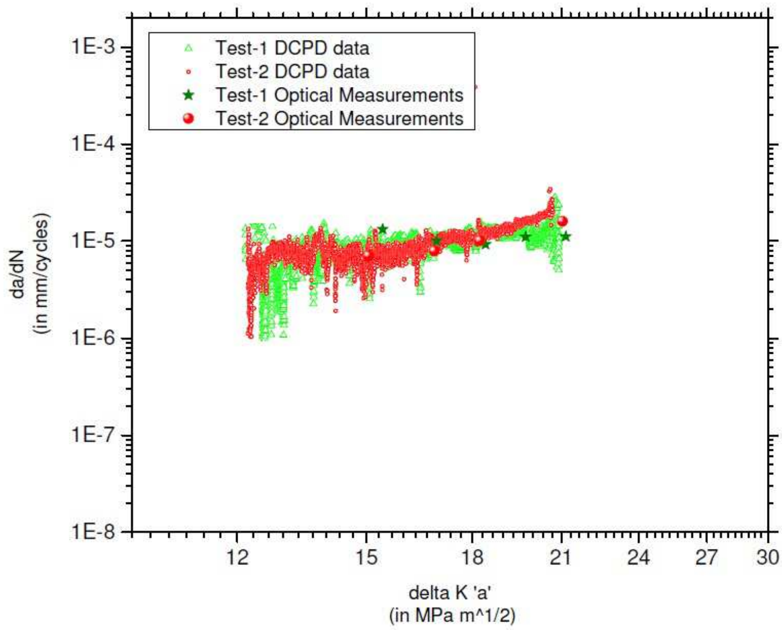

Figure 38 Figure shows comparison of the crack depth growth rates (da/dN) between pipe specimens without residual stress.

These curves are used to study the influence of thermally induced residual stresses on crack propagation behaviour of pipe specimens as discussed in Section 7.4 and Section 7.5. The curves are also used to compare crack propagation behaviour of pipe specimens with rectangular strip specimens to study the effects of scale and geometry on crack propagation behaviour as discussed in Section 7.7.

5 PIPE SPECIMEN WITH INDUCED RESIDUAL STRESS

In this chapter, the experimental data and results of constant amplitude fatigue tests on pipe specimens with residual stresses in notch region are discussed. In Section 5.1, the procedure used for generation of residual stress generation and the results from Finite Element simulation are explained briefly. In Section 5.2, the experimental data and results of constant amplitude fatigue tests are explained.

5.1 Residual Stresses

The primary objective of this research thesis is to study the effects of residual stress exclusively on fatigue crack growth rate in full scale pipes. To meet this objective, residual stress gradient is generated along the pipe wall thickness by fusion welding process at 23 mm distance from both sides of notch as shown in Figure 39. This is done to avoid influence on crack growth behaviour due to rough geometry, notches, porosity, phase changes during welding process and microstructure changes due to filler metal addition.

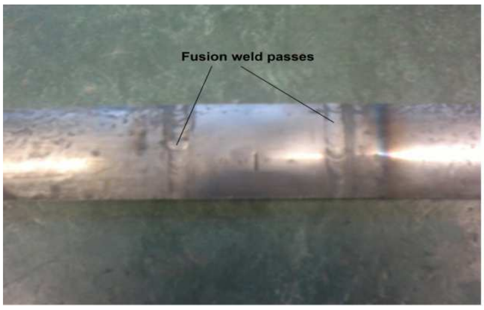

Figure 39 Figure shows the Fusion weld passes made at 23mm distance from both sides of notch to generate residual stress along pipe wall thickness

The parameters chosen for fusion welding are decided based on simulation results of FEM software Abaqus which is carried out by Allseas in Delft office. The parameters for welding are discussed in Section 3.4.2. Figure 40 shows the radial shrinkage of pipe wall at welded region. Linearly varying residual stresses from -170 MPa to +170 MPa are generated along wall thickness due to development of bending strains near the notch region(Appendix-D).

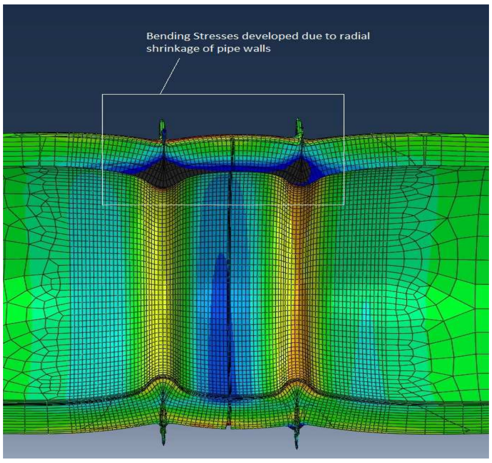

Figure 40 Figure shows FEM simulation on Abaqus showing bending in fusion weld zone due to radial shrinkage of pipe walls (100% magnification).

5.2 Constant Amplitude Fatigue Test

Two pipe specimens with residual stresses are tested under constant amplitude cyclic loads to investigate the crack growth behaviour in notched pipe specimen with induced residual stresses. The loading and environmental conditions are kept same as explained in Section 5.2. A strip specimen containing crack region extracted from the pipe specimen is broken to study the crack front shape change during fatigue test. It is found that the crack front grows in similar aspect ratio(a/c) compared to pipe specimen without residual stresses as shown in Figure 41. It could be due to reasons explained in Section 7.2.

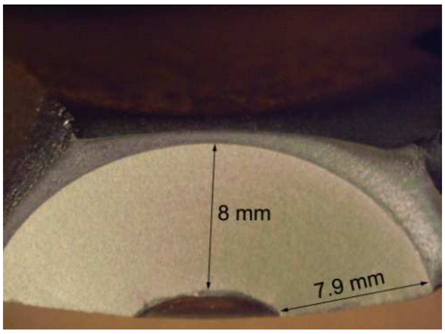

Figure 41 Figure shows crack front aspect ratio(a/c) at the end of fatigue test in pipe specimen with induced residual stresses

Optical measurements are taken for surface crack length measurements at various interval of cycles. The potential drop readings are noted from Howden machine corresponding to optical measurements. The data is used to prepare a calibration curve relating surface crack length with crack depth. This calibration curve is then used to calculate crack length(c) from the potential drop values collected from Howden potentiometer. The processing of potential drop data is performed as explained in Section 3.3.3. The processed data is then used for calculation of SIF range values and crack growth rate(da/dN) as illustrated in Section 5.2.

The experimental data may be used in different ways to study the crack propagation behaviour at various stages of fatigue test. The crack length 'c' vs. no. of cycles is plotted on log-log graph to study crack length propagation during fatigue test as shown in Figure 42. It is observed that slope of crack length growth increased steadily with number of cycles. It may be explained by the steady increase in stress intensity factor range with increasing crack growth during the test.

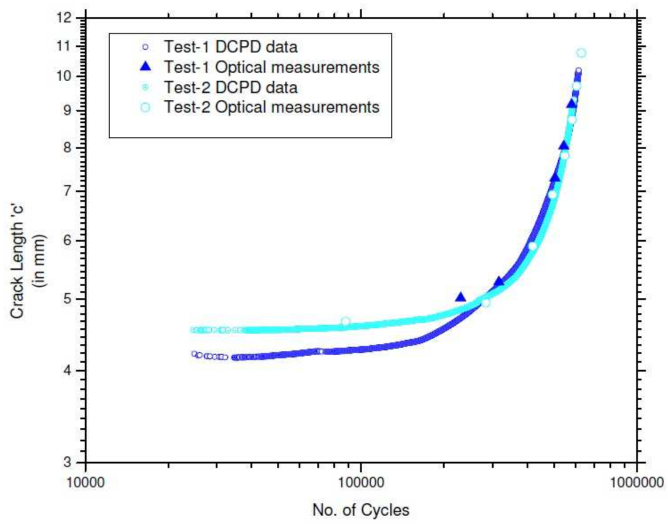

Figure 42 Figure shows comparison of Crack length (c) growth between pipe specimens with residual stress during fatigue test.

The crack depth 'a' vs. no. of Cycles is plotted on log-log scale in Figure 43 to study the crack depth growth with number of cycles. It is observed that crack depth increased steadily with number of cycles till it traversed mid-thickness of pipe wall. However, the crack depth growth decreased as it advanced towards back surface of pipe wall. It can be explained that the SIF value along depth increases less compared to SIF increase at the surface point as explained in Section 5.1.

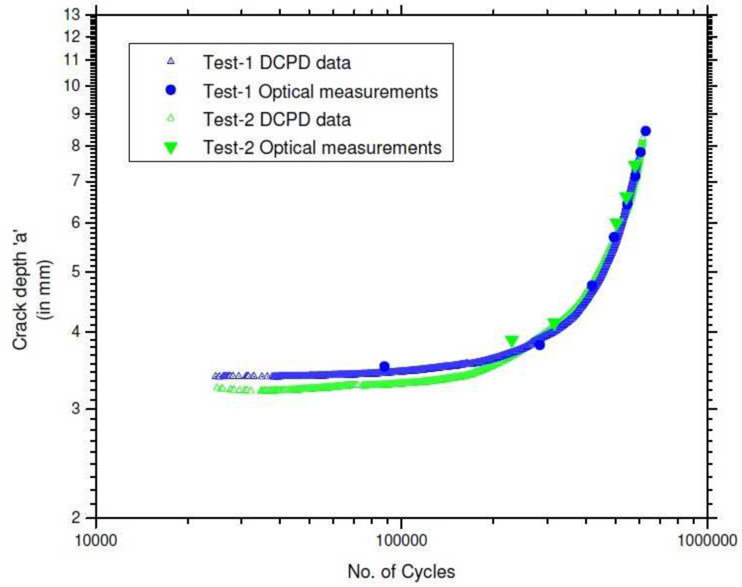

Figure 43 Figure shows comparison of crack depth (a) growth in pipe specimens with Residual Stress during fatigue test.

The surface crack growth rate(dc/dN) is plotted with respect to stress intensity factor range to study the crack growth behaviour along surface direction as shown in Figure 44.

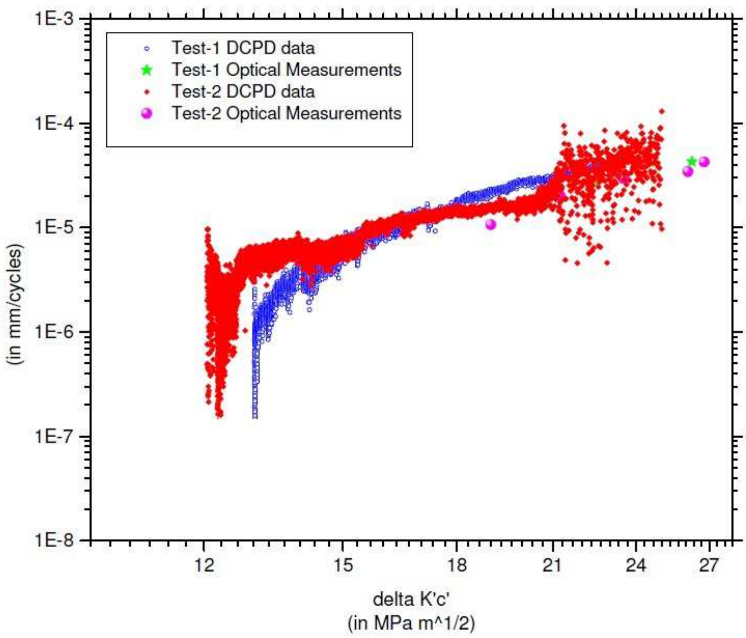

Figure 44 Figure shows Crack length growth rates(dc/dN) for pipe specimens with residual stress.

To study crack growth behaviour along depth direction, crack depth growth rate vs. SIF range is plotted in Figure 45. It can be seen that crack growth rate shows a linear increase with ΔK_a in the initial crack growth stage. However, a decrease in crack growth rate is observed as it advanced towards the back surface of the plate. It may be explained by the small increase in SIF range at this stage.

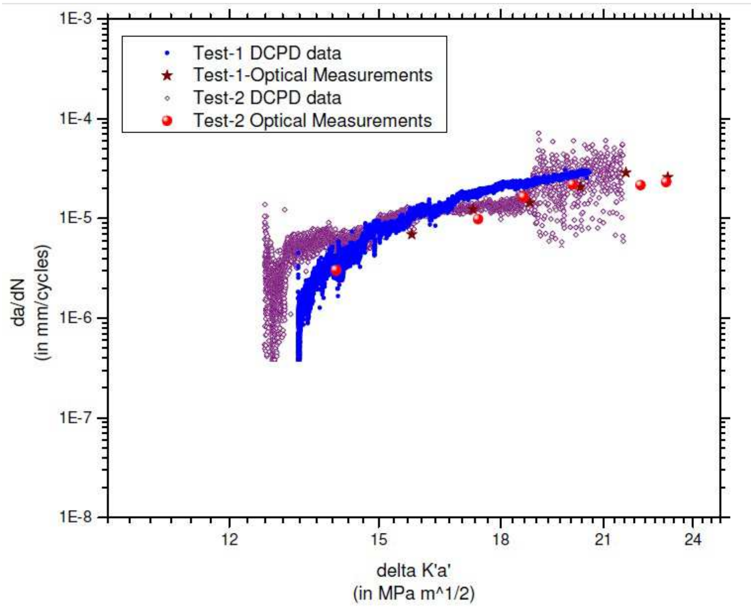

Figure 45 Figure shows crack depth growth rates(da/dN) for pipe specimens with residual stress.

6 STRIP SPECIMEN

In this chapter, the experimental data and results for three point bend tests on strip specimens are discussed. In Section 6.1, the loading conditions during fatigue test are briefly explained. Section 6.2 discusses the experimental data and results of single edge notch bend test (SENB).

6.1 Fatigue Test Parameters

The strip specimens are subjected to three point bend fatigue loading. The load range applied is 4.5KN which is decided on basis of similar tests performed by Allseas. The maximum load applied is 9.0KN and minimum load applied is 4.5 KN leading to a stress ratio(σ_{min}/ σ_{max}) of 0.5. As the load levels are low, the tests are performed at 30 Hz frequency. The environment for experiments was lab air of room temperature. There is always an uncertainty about crack initiation site in fatigue tests. To increase the probability of crack initiation at preferential position, a through thickness notch is machined in the strip specimen as discussed in Section 3.4.4.

6.2 Three Point Single Edge Notch Bend Test (3 SENB)

In three point bend test set-up, cyclic loads are applied by contact pins from the lower head of the MTS machine while the specimen is supported by one pin from upper side. This generates bending stresses in notch region. The three point bend test set-up is shown in Figure 46. Optical measurements are taken for every 1 mm crack length increase with respect to number of cycles and DCPD values. The potential probes and current electrodes are connected to the specimen for recording DCPD values as explained in Section 3.3.1. The data collected is then used to generate a calibration curve between the crack length and the potential drop values. Separate calibration curves are made for every strip specimen as the dimensions of both the strip specimens are different.

Figure 46 Three point bend fatigue test on notched strip specimen

There is always considerable noise in potential drop data collected due to the nature of fatigue tests and unavoidable external interferences with the potential drop signals. To make this data more comprehensible, the potential drop data is processed using adjacent averaging method as discussed in section 3.3.3. The processed data is then used for calculation of surface crack lengths.

The surface crack length data is used further for calculation of stress intensity factor (SIF) in accordance with ISO 12108 [34]. The stress intensity factor for maximum and minimum loads applied are calculated using following relationship [34]:

$$K = \frac{F}{BW^{1/2}} g(a/W) 10^{1.5}$$ Equation 24

where,

K = stress intensity factor(in $MPa/m^{1/2}$)

F = force applied (in KN)

B = thickness (in mm)

W = width (in mm)

a = crack length (in mm)

The stress intensity factor function, g (a/W), is calculated using following expression.

$$g(\frac{a}{W}) = \frac{6\alpha^{1/2}}{[(1+2\alpha)(1-\alpha)^{3/2}]}[1.99-\alpha(1-\alpha)(2.15-3.93\alpha+2.7\alpha^2)]$$ Equation 25

Here $\alpha = (a/W)$ for $0 \leq \alpha \leq 1.0$.

The Stress intensity factor range (ΔK_a) values are calculated by using the following relationship:

$$\Delta K_a = K_{max} - K_{min}$$ Equation 26

where,

K_{max} = maximum stress intensity factor

K_{min} = minimum stress intensity factor

The crack length data collected is then used to calculate crack growth rate (da/dN) by using following relation:

$$\frac{da}{dN} = (\frac{a_{i+1} - a_i}{N_{i+1} - N_i})$$ Equation 27

where,
a = crack length
dN =change in number of cycles
i = cycle number

The dc/dN Vs SIF range data is plotted on log-log scale for both strip specimens to study crack growth behaviour as shown in Figure 47.

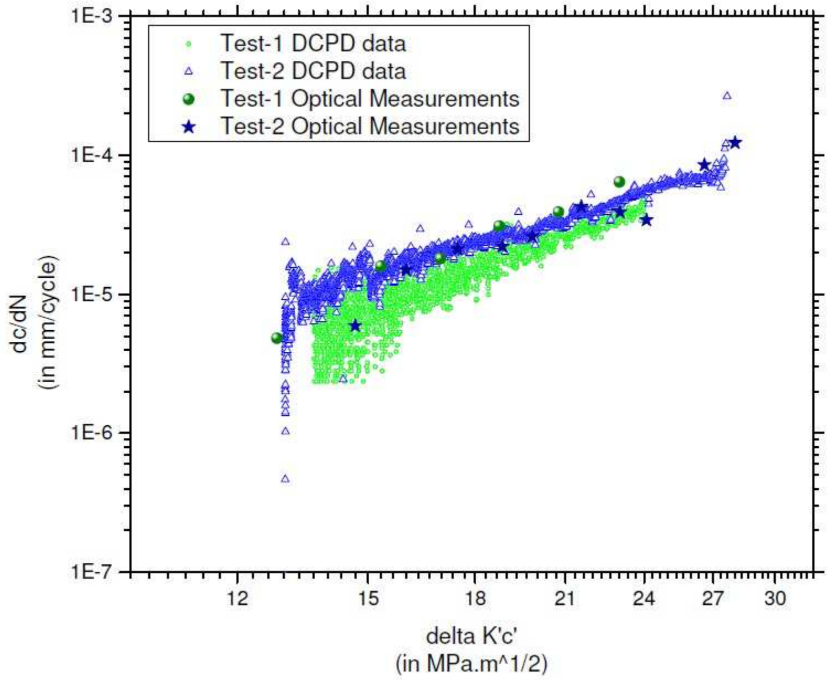

Figure 47 Figure shows crack length growth rates (dc/dN) for strip specimens.

7. DISCUSSION

In this chapter, results of fatigue tests on pipe specimens and strip specimens are studied and discussed. The main aspects related to experimental results discussed are following:

- Scatter in experimental data and error analysis.
- The factors affecting the crack front shape during crack propagation.
- Effect of residual stresses on mean stress and stress ratio.
- Local plastic deformation at crack tip in pipe with residual stresses.
- Effect of residual stress on crack growth rate in pipe specimens.
- Comparison of the crack length growth rates (dc/dN) for pipe specimens.
- Comparison of crack depth growth rates (da/dN) for pipe specimens.
- Effects of geometry and scale on fatigue crack growth rate.

7.1 Scatter In Experimental Data And Error Analysis

Scatter of fatigue life depends mainly on crack initiation period. If crack initiation can easily occur, scatter should be expected to be small [38]. In this research study, sharp notch is machined on specimens to reduce crack initiation period and hence small scatter is expected for fatigue crack growth in pipe specimens. Two specimens for each test condition of a test program may be sufficient, if they show quantitatively the same crack growth. In this research, the results corresponding to same test condition are found to be similar and shows small scatter as shown in chapter 4, 5 and 6. However, there are other possible sources for scatter in fatigue results like change in environmental conditions, and slight difference in specimens position on Test-Rig. To take into account the scatter involved due to these factors, regression analysis is used. The values for particular parameter for tests corresponding to same test condition are averaged and a line curve is then fitted through averaged data points. The square of residual is kept maximum through iterative convergence. The upper and lower 99% prediction bands are then calculated for the likely interval of this curve.

7.2 Effect Of Aspect Ratio(a/c) & Thickness On Crack Propagation

Variable amplitude fatigue test was performed to study and compare the crack length position and crack depth position at progressive cycle numbers during fatigue test as discussed in Section 4.1. The initial aspect ratio (a/c) of semi-elliptical notch in pipe specimen was 0.25. During initial crack growth stage, outward crack increment was not uniform along the crack perimeter. Crack front grew faster in crack depth direction than circumferential direction as shown in

Figure 48. The crack front propagation shows this tendency because stress intensity factor (K_{max}) varies along the crack front perimeter and is maximum at the crack tip ($\varphi = 90^0$) along depth direction and minimum at crack tip on surface during the early phase of crack propagation.

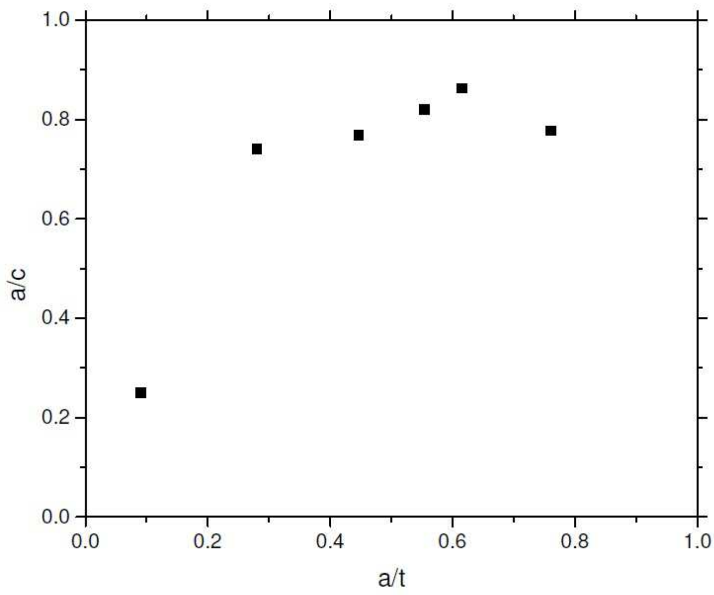

Figure 48 Variation of crack aspect ratio(a/c) with depth/thickness(a/t) ratio.

Another reason for such crack front shape might be the presence of plane stress conditions at the surface crack tip and plane strain conditions at crack tip in depth direction. Plane strain conditions at the crack tip are due to presence of tri-axial state of stress at the crack tip. It leads to larger plastic wake at surface crack tip and smaller plastic wake at crack depth tip as shown in Figure 49. Plastic yielding is spread over a larger area on pipe surface while in crack depth direction, plastic yielding is localised. Due to this, magnitude of plastic yielding at crack tip on the surface is smaller compared to plastic yielding at crack tip along depth direction. It leads to faster crack growth rate in depth direction compared to the surface during initial crack growth phase.

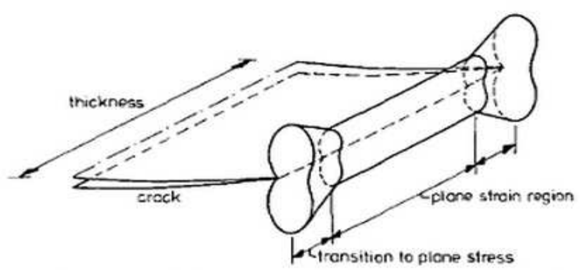

Figure 49 Plastic wake size distribution along crack perimeter[Source: [39]]

This is further supported by results from numerical analysis by X.B Lin (et al.) [40], as shown in Figure 50.

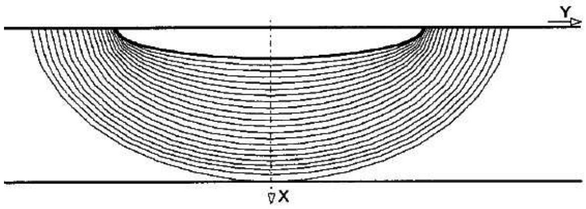

Figure 50 Figure shows crack front shape changes during fatigue crack propagation. The crack front grew more in depth direction as compared to surface direction [40].

It is observed that the SIF values become approximately equal when a/c ≈ (0.72-0.82) which is in agreement with numerical results by X.B Lin (et al.) [41]. After reaching iso-K ($K_a \approx K_c$) ratio, crack front grows uniformly along the circumferential and depth directions as shown in Figure 49. At a/t ratio of 0.65, the crack growth rate at surface becomes more than crack growth rate along depth direction. It is because the SIF value at the deepest point for bending increases slowly whilst the SIF value at surface point increases significantly due to bending load [41].

7.3 Effect Of Residual Stresses On Mean Stress And Stress Ratio

A residual stress gradient is generated along pipe wall thickness using fusion welding as discussed in Section 5.1. The presence of residual stresses does not influence the magnitude of stress intensity factor range(SIF). However, the residual stress increases the mean stress(σ_m) value and stress ratio(R) significantly. It will also increase K_{min} due to which the crack might remain in open state for longer time/loading cycle or for entire loading cycle. The effective stress intensity factor range(ΔK_{eff}) will be more than SIF range for pipe specimen without residual stresses. So, it is expected to increase the crack propagation rate in pipe specimens with induced residual stresses as observed in Sections 7.5 and 7.6.

7.4 Local Plastic Deformation At Crack Tip In Pipe With Residual Stress

The plastic deformation zone at crack tip influences crack growth rate significantly during crack growth stage. Plastic deformation zone is formed when the stresses developed at crack tip exceeds the yield strength of material. The presence of induced residual stresses can have significant influence on size of plastic deformation zone formed at crack tip during fatigue loading [42]. To investigate the formation of plastic deformation, strain gauges were used to measure the uni-axial tensile stresses generated on the pipe surface and to check if plastic yielding takes place on load application. In this test, a strain gauge was glued onto the pipe surface at 90 degree from the notch region. This was done to avoid any stress reduction which is expected at notch region.

The maximum tensile stress generated on 300 KN (upper load limit) load application is found to be 342 MPa during first load cycle shown in Figure 46 . However, a maximum load of 330 KN is applied on the pipe specimen during first load cycle. The maximum stress generated is found to be 337 MPa by the strain gauge. On load removal, the stress value is reduced to 5.6 MPa. This shows the occurrence of plastic yielding on pipe surface. It might be explained by the presence of tensile residual stresses developed on pipe surface during the fusion welding. The combined tensile stresses developed due to residual stress and external load application might have exceeded the yield strength of pipe material. A larger plastic deformation could be expected at notch tip due to the fact that presence of sharp notch tip will increase the stress concentration as shown in Figure 51.

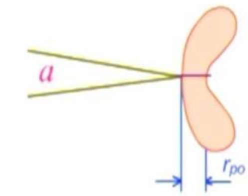

Figure 51 Plastic deformation zone during first load cycle. (Source: NPTEL [44])

The radius of plastic deformation region($2*r_{po}$) for both test conditions can be calculated by Equation 28 proposed by Irwin [43].

CASE I: For pipe specimens with residual stresses

$$2*r_{po} = \frac{1}{\pi}\left(\frac{K_{max}}{\sigma_y}\right)^2 \quad \text{Equation 28}$$

$$2*r_{po} = \frac{1}{\pi}\left(\frac{27.5}{540}\right)^2$$

$$2*r_{po} = 0.83 \text{ mm.}$$

Here, K_{max} is maximum stress intensity factor at crack tip and σ_y is yield strength of pipe material.

CASE II: For pipe specimens without residual stresses

$$2*r_{po} = \frac{1}{\pi}(\frac{K_{\max}}{\sigma_y})^2$$

$$2*r_{po} = \frac{1}{\pi}(\frac{17.5}{540})^2$$

$$2*r_{po} = 0.03 \text{ mm.}$$

The same load cycle is applied again to check for plastic yielding. In the subsequent load cycles, no further plastic deformation is observed for same load range as shown in Table 3. It shows slight relaxation of residual stresses during plastic yielding. The experimental readings of strain gauge between uni-axial stress and load applied are shown in Figure 52. It shows a linear relationship between loads applied and the uni-axial stress generated. The maximum permissible percentage of strain for strain gauge used is 2.8% which is higher than the strain generated during the test.

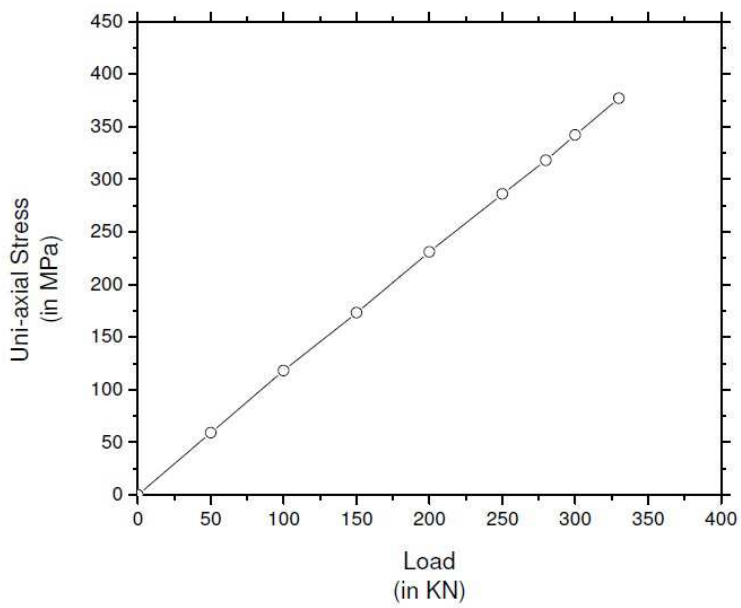

Figure 52 Load and stress variation during first static load cycle

S. No.	Applied Load (In KN)	Stress Value (In MPa)
First Cycle		
1	0	0
2	50	59
3	100	118
4	150	173
5	200	231
6	250	286
7	280	318
7	300	342
8	330	377
9	0	5.6
Second Cycle		
1	0	5.6
2	300	340.6
3	0	5.6

Table 3 Experimental readings obtained from strain gauge showing uni-axial stress variation with loads applied.

7.4 Effect Of Residual Stress On Crack Growth Rate In Pipe Specimens

The experimental results of full scale fatigue tests on pipe specimens are compared to analyze the influence of induced residual stresses on crack growth as shown in Figure 53. It is observed that the slope of crack growth for pipe specimens with induced residual stresses was smaller than slope of crack growth for pipe specimens without residual stresses during initial crack growth stage.

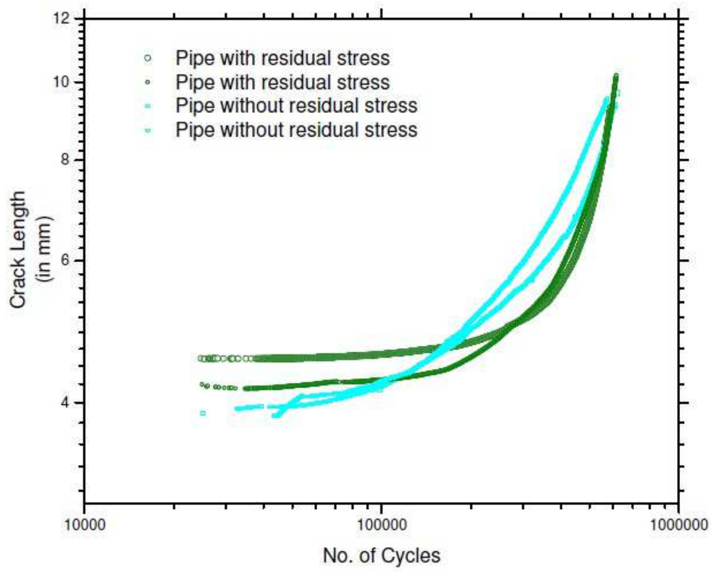

Figure 53 Comparison of crack length(c) growth curves for all pipe specimens

It could be due to the presence of plastic deformation zone at crack tip formed during first load cycle as explained in Section 7.3. When the crack was traversing through this large plastic deformation zone, the crack tip would experience additional compressive stresses, shown in Figure 54.

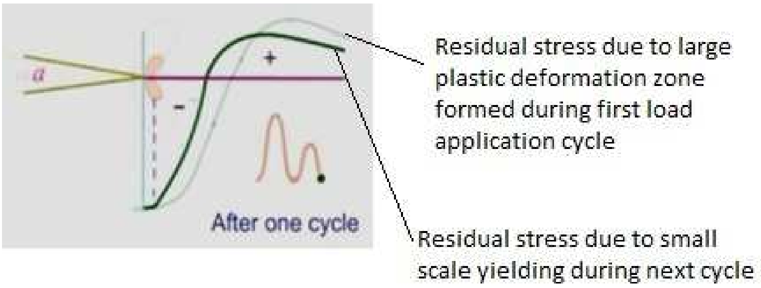

Figure 54 Figure shows the compressive residual stresses experience at crack tip during crack Propagation through larger plastic deformation zone [Source: NPTEL [44]].

At zero load, the crack tip would experience compressive stresses. When the external load is applied, crack tip would open fully only when tensile stresses generated would become greater than these compressive stresses. Thus, the residual compressive stresses at crack tip will reduce the effective tensile stress magnitude as shown below:

Effective tensile stress = Tensile stress - Compressive stress.

It would reduce the effective stress intensity factor range and thus retard crack growth rate in this zone as shown in Figure 55.

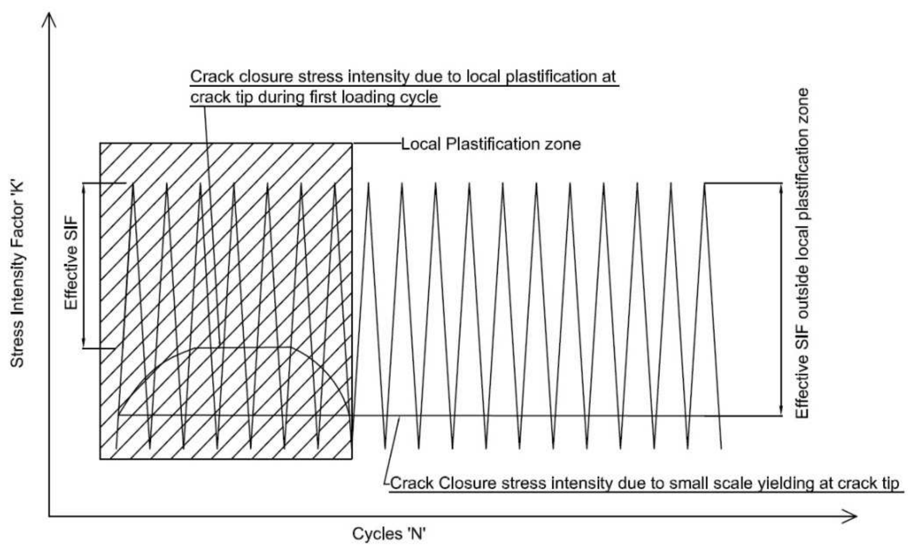

Figure 55 Figure shows stress intensity factor variation during fatigue test in pipe specimens with residual stresses.

As the crack tip grows further, it wades out of this plastic deformation zone. The crack growth is then expected to be mainly influenced by two factors: elastic stress field(SIF) and small scale yielding present at the crack tip. In fatigue crack propagation, there is a high stress concentration near the crack tip due to sharp geometry. Therefore, small scale yielding is expected at crack tip on load application as shown in Figure 56 which is a typical phenomenon for ductile materials.

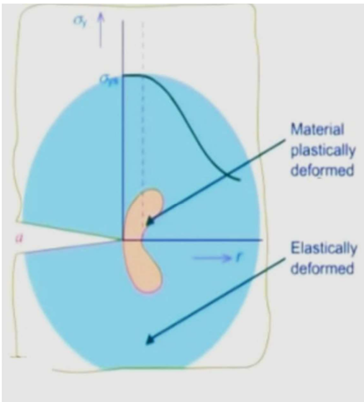

Figure 56 Small scale yielding at crack tip [Source: NPTEL [44]]

Due to small scale yielding at crack tip, some compressive residual stresses will be present at crack tip as shown in Figure 57. These compressive residual stresses will decrease the effective SIF range and decrease the crack growth rate shown in Figure 55. So, the crack propagation rate is lower as is expected in presence of elastic stress field alone. Another reason for it might be the partial relaxation of residual stresses during crack propagation [27].

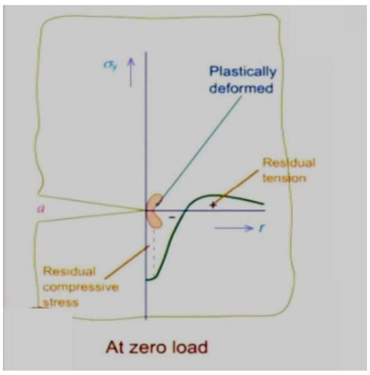

Figure 57 Residual stress distribution at crack tip at zero load condition. [Source: NPTEL [44]]

7.5 Comparison Of Crack Length Growth Rates For Pipe Specimens

The crack length growth(dc/dN) data is plotted with respect to ΔSIF values to study the influence of residual stresses on crack length propagation as shown in Figure 58 and Figure 59. Not all data values are considered to plot this curve. The data set is split into different regions with a intention to study the mechanism dominating in that region. Crack front is in stable aspect ratio of 0.72-0.82 and has already traversed through the plastic deformation zone formed during first load cycle in the data set considered.

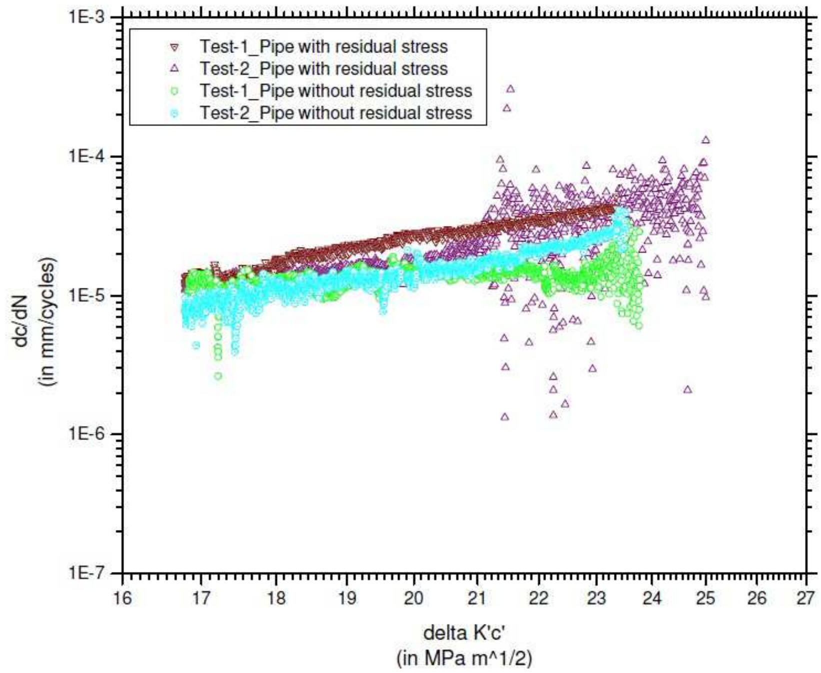

Figure 58 Comparison of dc/dN Vs Delta k_c curves between all pipe specimens

It is observed that crack length growth rate(dc/dN) for pipe specimens with induced residual stresses is higher than crack length growth rate for pipe specimens without induced residual stresses. It might be because the stress intensity factor(K_{max} & K_{min}) at crack tip for pipe specimens with induced residual stresses is higher than SIF(K_{max} & K_{min}) for pipe specimens without induced residual stresses. The crack tip would remain in fully open state during whole loading cycle as discussed in Section 7.2. Thus, the effective stress intensity factor range(ΔK_{eff}) would be higher for pipe with residual stresses as compared to pipe without residual stresses.

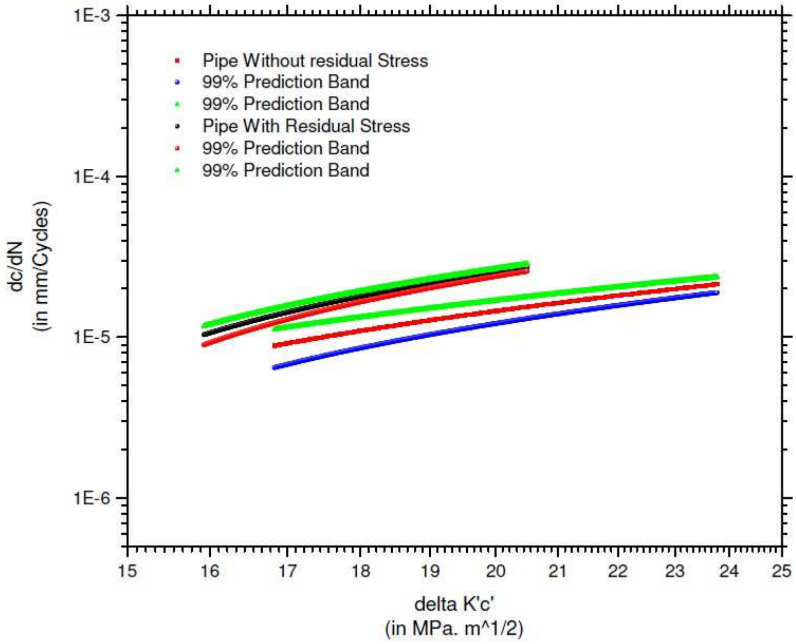

Figure 59 Line curve is drawn for two test conditions as discussed in section 7.1. Prediction bands with 99% interval are calculated to show the possible scatter in the results.

7.6 Comparison Of Crack Depth Growth Rates For Pipe Specimens

There are many factors which could lead to difference in crack growth rate along depth direction from crack growth rate along surface direction. These are as following:

- Presence of Plane Stress conditions on surface and plain strain conditions along depth direction [39].
- A constant residual stress is generated along surface while a linearly varying residual stress gradient is generated along pipe wall thickness during the heat treatment of pipe specimens by fusion welding.
- Crack depth growth rate(da/dN) slows down as it advances towards back surface of plate due to reduction in ΔK_a values while crack length growth(dc/dN) rate is influenced by constantly increasing ΔK_c values [41].

Due to these differences, it is important to study the crack depth growth rates(da/dN) for pipe specimens without residual stresses and pipe specimens with induced residual stresses. To investigate this, the da/dN curve is plotted as a function of ΔK values as shown in Figure 60 and Figure 61.

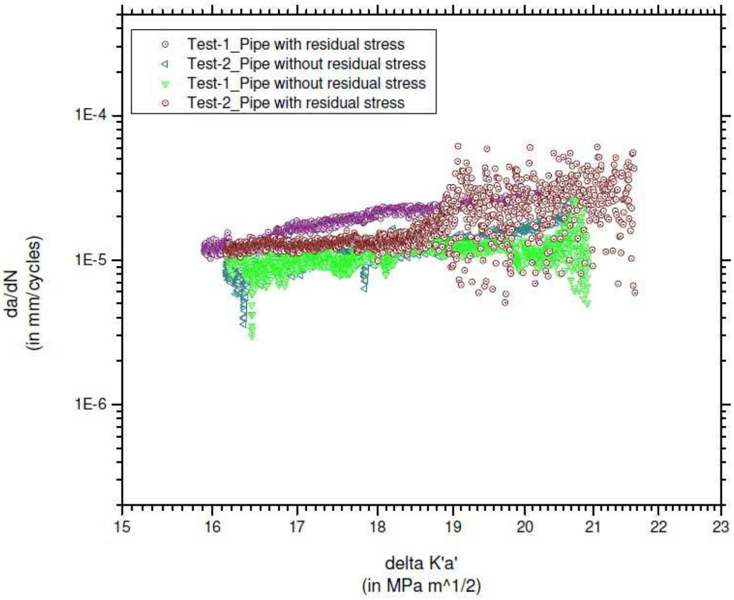

Figure 60 Comparison of da/dN with ΔK_a curves between all pipe specimens

The data set is again split into different regions with a intention to study the mechanism dominating in that region as explained in Section 7.5. On comparison of crack depth growth rate curves, it is found that crack growth rate for pipe specimens with induced residual stresses is higher compared to crack growth rate for pipe specimens without induced residual stresses. It could be explained by the similar justification provided in Section 7.5 and 7.2.

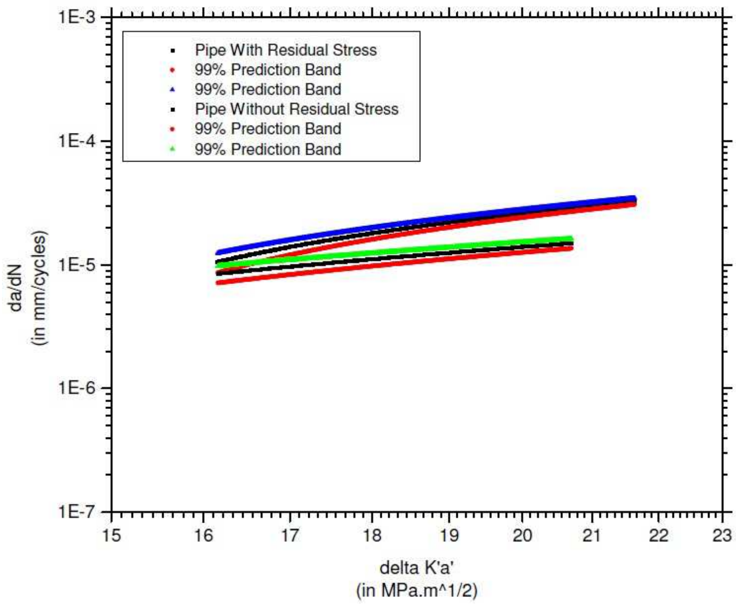

Figure 61 Line curve is drawn for two test condition as discussed in section 7.1. Prediction bands with 99% interval are calculated to show the possible scatter in the results.

7.7 Comparison Of Crack Growth Rate Of Pipe Specimens And Strip Specimens

The results of crack length growth rate(dc/dN) with respect to ΔK_c are plotted for pipe specimens without residual stresses and strip specimens extracted from pipe specimens. It is observed that the crack length growth rate(dc/dN) for strip specimens is comparable to crack length growth rate for pipe specimens during most portion of fatigue test, as shown in Figure 62 and Figure 63.

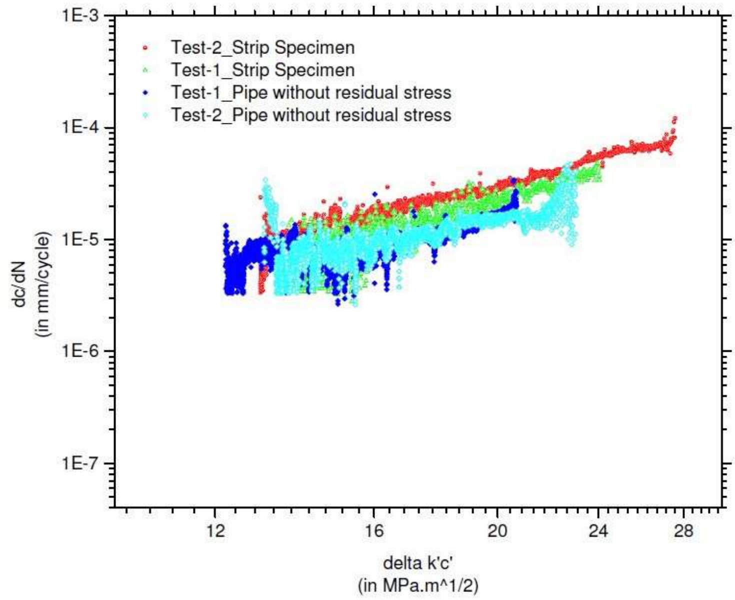

Figure 62 Figure shows comparison of crack length growth rates(da/dN) between pipe specimens and strip specimens.

As the crack progressed, the crack growth rate in the strip specimen became faster in strip specimens compared to pipe specimens. It might be due to the fact that relative plasticity developed at the crack tip in strip specimens is comparatively higher than relative plasticity at crack tip in pipe specimens during later portion of fatigue test.

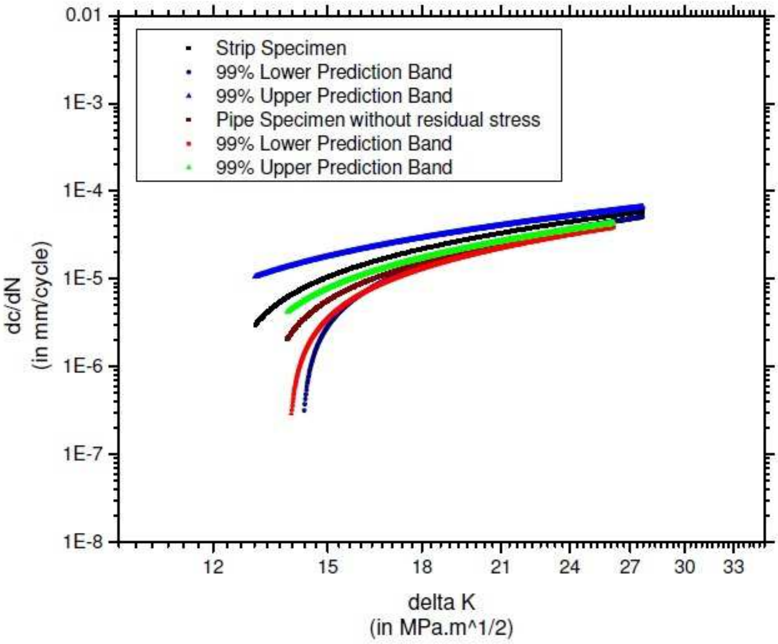

Figure 63 Figure shows the comparison between crack growth rate between strip specimens and pipe specimen using curve fitting.

8 CONCLUSIONS

8.1 Effect Of Aspect Ratio And Thickness On Crack Front Shape

- The crack front shape is guided by the aspect ratio (a/c) of surface flaw. The surface crack has a tendency to grow with aspect ratio of 0.70-0.82 for small initial a/t ratio. The crack growth rate along the depth and surface varies till a/c ratio reaches this range. In this study, initially crack depth growth rate (da/dN) was comparatively higher than crack length growth rate (dc/dN) due to notch aspect ratio of 0.25.

8.2 Effect Of Residual Stress On Crack Growth Rate

- Residual stresses slightly slows down crack growth rate during initial crack growth stage. A larger plastic deformation zone is formed at crack tip during first load cycle. It might be due to the reason that crack has to wade through this plastic deformation zone during which crack tip experiences residual compressive stresses which decrease the effective SIF range.

- In the mid-thickness region, the crack growth rate for pipe specimens with residual stresses is slightly higher than crack growth rate for pipe specimens without residual stresses. It might be because of the increase in maximum stress intensity (K_{max}) at the crack tip due to residual stresses .

8.3 Difference Between Crack Depth Growth Rate And Crack Length Growth Rate

- The crack length growth rate (dc/dN) increases steadily during fatigue test while crack depth growth rate varies during fatigue test. It is because the SIF value at crack tip on surface increases steadily with crack propagation while SIF value at crack depth tip remains constant due to global plasticity as it advances towards back surface of pipe wall.

8.4 Difference Between Crack Growth Rate Of Strip Specimen And Crack Growth Rate Of Pipe Specimen

- The crack length growth rate for strip specimens is comparable to crack length growth rate for pipe specimens during a large portion of fatigue test.

8.5 Fatigue Tests For Full Scale Pipe Specimens Using Four Point Bending Set-up

- Four point bend test-rig can be used to perform full scale pipe specimens fatigue tests. Beachmarks can be used as an important tool to monitor crack depth along with surface crack measurements. The reliability of the results can be increased by using DCPD method in combination with optical measurements.

- Automated crack length measurements can be taken using Direct Current Potential Drop method reliably for four point full scale fatigue tests.

9 RECOMMENDATIONS AND ASSUMPTIONS

9.1 RECOMMENDATIONS

Following recommendations can be considered for further studies on the basis of this research.

- Two tests are performed for each test condition due to the time taken per experiment and time constraints of this thesis study. Since scatter is inherent characteristics of fatigue tests. Additional experimental work can be done to investigate the scatter behaviour to draw solid conclusions.

- At high external loads, there will be considerable plastic deformation during first loading cycle at flaw tip in materials with residual stress. It is observed in this research study that similar plastic deformation helps in increasing the fatigue strength. It might produce the same favorable effect of plastic deformation by shot peening which is generally used to increase fatigue strength of structures. Hence, shot peening might not be a cost effective solution for materials used under high external loads. Further experimental investigation in this direction can lead to more conclusive results.

- The design of test-rig was guided by space constraints of MTS machine used in this research study. Test-rig design could be improved by creating more space to take optical measurements without disturbing the specimens. It will eliminate the jumps in DCPD data occurred while taking optical measurements which could increase the reliability of the potential drop data.

- In this thesis study , initial aspect ratio of semi-elliptical notch was 0.25. It is observed that crack depth grew faster compared to surface crack length during initial fatigue crack propagation. Significant literature is present to provide the evidence of such crack growth in plate specimens. Further tests can be performed for different aspect ratios to analyze the effect of initial aspect ratio on difference in crack depth growth rate and crack length growth rate in pipe specimens.

9.2 ASSUMPTIONS

Following assumptions and approximations are used during analysis and interpretation of data.

- The maximum temperature reached in the notch region is 300^{o}C during the fusion welding process. So, there is no phase transformation in notch region due to fusion welding process.

- The scale of SIF range chosen for analysis of results is small (15-30 MPa.m$^{1/2}$) compared to scale (1-100 MPa.m$^{1/2}$) used in codes (BS7910). This is done to magnify the difference in crack growth rates which could become invisible if large scale for SIF range is chosen during analysis of results.

- Redistribution of residual stresses takes place during crack propagation as discussed in literature review. However, it is difficult to measure residual stresses during fatigue tests. Therefore, residual stress redistribution during fatigue test is not included in analysis of data.

10 BIBILOGRAPHY

[1] "Pipeline Transportation Systems for Liquid Hydrocrbons and Other Liquids," ASME Code for Pressure Piping, 2009.

[2] "EN 1993 1-9 Design of Steel structures : Fatigue strength of steel structures," 1993.

[3] "Guide to methods for assessing the acceptability of flaws in Metallic Structures," British Standards, 2005.

[4] M. Siddique, "Experimental and Finite Element Investigation of Residual Stresses and Distortions in Welded Pipe-Flange Joints," 2005.

[5] C. P. A. Bathias, Fatigue of Materials and Structures - Fundamentals, John Wiley & Sons., 2010, p. Page 6.

[6] P. Paris, "A Critical Analysis of Crack Propagation Laws," *Journal of Basic Engineering,* pp. 528-534, 1960.

[7] K. Sobczyk, "Fatigue crack growth in random residual stresses," *International journal of fatigue,* pp. 1179-1187, 2004.

[8] "Good Design Practice - A Guideline for Fatigue Design," European Convention for Constructional Steelwork - Technical Committee 6 , 2000.

[9] J. K. a. R. J. C. MUSUVA, "THE EFFECT OF STRESS RATIO AND FREQUENCY ON FATIGUE CRACK GROWTH," *Fatigue & Fracture of Engineering Materials & Structures,* p. 457–470, (1979).

[10] W. Fricke, "http://www.woodheadpublishingonline.com," [Online]. [Accessed Sunday, June 02, 2013 4:28:18 AM June 2013].

[11] M. Ashby, Materials engineering, science, processing and design, Butterworth-Heinemann, 2010.

[12] D. C. M. Radaj, Fatigue assessment of welded joints by local approaches, Cambridge: Abington Publishing, 1998.

[13] "ESDEP- The European Steel Design Education Programme - Lecture WG 12 - Fatigue".

[14] W. J, "Hollow Section Joints," Delft University Press, 1982.

[15] L. e. a. Satyarnarayan, "FATIGUE CRACK GROWTH MEASUREMENTS USING ULTRASONIC AND ACPD TECHNIQUEs FOR STAINLESS STEEL PIPES".

[16] R. Pijpers, "Fatigue strength of welded connections made of very high strength cast and rolled steels," 2011.

[17] H.-M. &. S. K.-H. Bauschke, "Measurement of the depth of surface cracks using the direct current potential drop method," *Materialwissenschaft und Werkstofftechnik,* vol. 16, no. 5, pp. 156-165, 1985.

[18] A. DeBiccari, "Control of distortion and residual stresses in girth welded pipes," Massachusetts Institute of Technology, 1986.

[19] R. Leggatt, "Residual stresses in welded structures," *International Journal of Pressure Vessels and Piping,* vol. 85, no. 3, pp. 144-151, 2008.

[20] M. N.-P. T. a. D. K. Faraijian, "Relaxation of welding residual stresses - Part I: under quasi-static loading," *Int. J. Microstructure and Materials Properties,* vol. 7, no. 1, pp. 3-15, 2012.

[21] R. Mattson and W. Coleman, "Effect of Shot-Peening Variables and Residual Stresses on the Fatigue Life of Leaf-Spring Specimens," *SAE Technical Paper,* 1954.

[22] S. Kodama, "The behavior of residual stress during fatigue stress cycles," in *Proceeding of the International Conference on Mechanical Behavior of Metals (ICMBM'72)*, 1972.

[23] M. &. D. K. Farajian-Sohi, "RESIDUAL STRESS RELAXATION IN WELDED JOINTS UNDER STATIC AND CYCLIC LOADING".

[24] A. N. S. a. Y. M. Ohta, "Unique fatigue threshold and growth properties of welded joints in a tensile residual stress field," *International journal of fatigue,* pp. 303-310, 1997.

[25] R. C. McCLUNG, "A literature survey on the stability and significance of residual stresses during fatigue," *Fatigue & Fracture of Engineering Materials & Structures,* vol. 3, p. 173–205, 2007.

[26] C. D. M. e. a. Liljedahl, "The effect of weld residual stresses and their re-distribution with crack growth during fatigue under constant amplitude loading," *International*

Journal of Fatigue, pp. 735-743, 2010.

[27] M. K. K. a. K. I. Takanashi, "Relaxation behavior of welding residual stresses by fatigue loading in," *Welding World,* vol. 44, p. 28–34, 2000.

[28] S. a. Y. T. FUKUDA, "An experimental study of redistribution of welding residual stress with fatigue crack extension," *Transactions of JWRI 7.2,* pp. 215-220, 1978.

[29] R. a. A. L. Galatolo, "Fatigue crack propagation in residual stress fields of welded plates," *International Journal of Fatigue,* pp. 43-49, 1997.

[30] Y. C. a. K. S. L. Lam, "The effect of residual stress and its redistribution of fatigue crack growth," *Theoretical and Applied Fracture Mechanics ,* pp. 59-66, 1989.

[31] "The effect of weld residual stresses and their re-distribution with crack growth during fatigue under constant amplitude loading," *C.D.M. Liljedahl, O. Zanellato, M.E. Fitzpatrick, J. Lin, l. Edwards,* vol. 32, no. 4, pp. 735-743, 2010.

[32] Y. M. S. S. A. Zhang, "Re-evaluation of fatigue curves for flush ground girth welds," *Tubular Structures XII: Proceedings of Tubular Structures XII,* p. 341, 2008.

[33] A. F. Liu, "Mechanics and mechanisms of fracture: an introduction," *ASM International,* pp. 133-134, 2005.

[34] "ISO 12108-Metallic Materials- Fatigue Testing-Fatigue crack growth method," Insternational Organisation for Standardisation, 2002.

[35] A. a. M. A. M. Hosseini, "Evaluation of stress intensity factor and fatigue growth of surface cracks in tension plates," *Engineering fracture mechanics,* pp. 957-974, 1985.

[36] M. A. a. A. H. Mahmoud, "Assessment of stress intensity factor and aspect ratio variability of surface cracks in bending plates," *Engineering fracture mechanics,* vol. 24.2, pp. 207-221, 1986.

[37] J. R. I. Newman Jr., "An empirical stress-intensity factor equation for the surface crack," *Engineering Fracture Mechanics,* vol. 15, no. 1-2, pp. 185-192, 1981.

[38] J. Schijve, Fatigue of Structures and Materials, Springer.

[39] J. Schijve, "Fatigue Crack Closure: Observations and Technical Significance," in *Mechanics of Fatigue Crack Closure*, 1988, p. 12.

[40] X. B. a. R. A. S. Lin, "Finite element modelling of fatigue crack growth of surface cracked plates: Part II: Crack shape change," *Engineering Fracture Mechanics,* vol. 63.5, pp. 523-540, 1999.

[41] X. B. a. R. A. S. Lin, "Finite element modelling of fatigue crack growth of surface cracked plates: Part III: Stress intensity factor and fatigue crack growth life.," *Engineering Fracture Mechanics,* vol. 63.5, pp. 541-556, 1999.

[42] J. Baumgartner, "Enhancement of the fatigue strength assessment of welded components by consideration of mean and residual stresses in the crack initiation and propagation phases," in *International Institute of Welding*.

[43] G. Irwin, "Analysis of stresses and strains near the end of a crack traversing a plate," *Journal of Applied Mechanics,* vol. 24, pp. 361-364, 1957.

[44] K. Ramesh, "NPTEL E-Learning Courses from IITs and IISCs," [Online].

[46] M. Siddique, "Experimental and Finite element investigation of residual stresses and distortions in welded pipe-flange joints".

[47] K. S. Y. a. M. T. Iida, "Residual stress relaxation by reversed loading.," *Welding in the World/Le Soudage dans le Monde,* pp. 138-144, 1997.

[48] "Guide to methods for assessing the accpetability of flaws in metallic structures," British Standards, 2005.

[49] S. J. Maddox, "Review of fatigue assessment procedures for welded aluminium structures," *International Journal of Fatigue,* vol. 25, no. 12, pp. 1359-1378, 2003.

APPENDIX-A

Calculation of Beam test-frame according to NEN6770:1997

$F_{v;rep}$	300	kN
lf	1	
F_d	300	kN

Assumption: all points work as hinge

Beam at two endsupports							
ctc support		l	550	mm			
Occuring moment		$M_{y;s;d}$	41.25	kNm			
Shearforce		$V_{z;d}$	150	N			
Material Beam	S355	$f_{y;d}$	355	N/mm^2			
		E_d	210000	N/mm^2			
Required Modulus		$W_{y;d}$	116197	mm^3			
Type Profile	HEB200B						
Modulus		$W_{y;el}$	569600	mm^3	OK		
Moment of Inertia		$I_{y;el}$	56960000	mm^4			
Profile height		h	200	mm			
Profile width		b	200	mm			
Section		A	7810	mm^2			
Area web		A_w	2485	mm^2			
Flange width		tf	15	mm			
Web thicknes		t_w	9	mm			
Radius		r	18	mm			
Profile heigth		h	200	mm			
Allowable Moment		$M_{y;el;d}$	202.2	kNm	OK		
Allowable Shear		$V_{z;el;d}$	509.3	kN	OK		

Capacity of Web

					UC		
Capacity	Endsupport	$F_{u;1;d}$	303.9	kN		0.49	OK
Influence of end distance to loadpoint		d_1	36.1	mm			
	Support	$F_{u;1;d}$	630.8	kN		0.24	OK
		d_1	138.4	mm			
	Occuring tension	σ_b	72.4	N/mm^2			
	Area of influence	c	59	mm			

Local buckling of web Support

Capacity	Support	$F_{u;2;d}$	172.4	kN		0.87	OK

Global buckling of web

Capacity	**Support**	$F_{u;3;d}$	326	kN	0.46	OK
	Effective width	bef	154.7	mm		
	buckling length	h_{buc}	200.0	mm		
	support length	c	90.0	mm		
	Moment of inertia	Iy	9395.5	mm^4		
	Area	A	1391.9	mm^2		
	radius of gyration	iy	2.6	mm		
	Euler slenderness	λ_e	76.4			
	Buckling slenderness	λ_y	77.0			
	relative slenderness	$\lambda_{y;rel}$	1.01			
	Euler-buckling force	$F_{y;E}$	486.8	kN		
	buckling factor	ω_{buc}	0.66			
		α_k	0.21			
		λ_o	0.2			

Unity Check	Middle support	
14.2-1	0.9	OKt
	Endsupport	
14.2-1	0.9	OKt
14.2-2	Middle support	
	0.72	OKt

APPENDIX-B : PIPE DATA SHEET

The dimensions and material properties used in calculation for this research are taken from inspection certificate of pipe shown below.

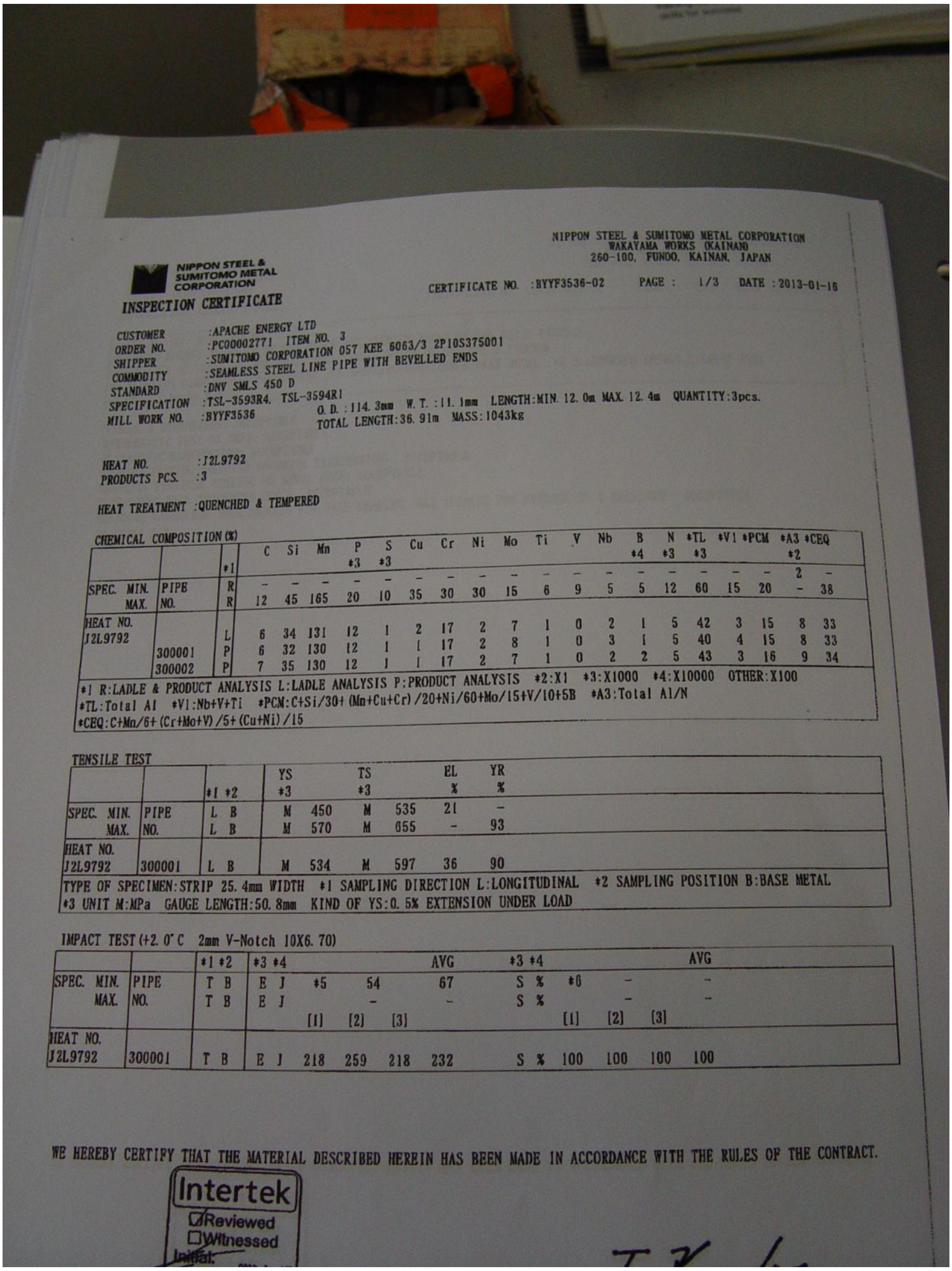

NIPPON STEEL & SUMITOMO METAL CORPORATION
WAKAYAMA WORKS (KAINAN)
260-100, FUNOO, KAINAN, JAPAN

NIPPON STEEL & SUMITOMO METAL CORPORATION

INSPECTION CERTIFICATE

CERTIFICATE NO. :BYYF3536-02 PAGE : 1/3 DATE :2013-01-16

CUSTOMER :APACHE ENERGY LTD
ORDER NO. :PC00002771 ITEM NO. 3
SHIPPER :SUMITOMO CORPORATION 057 KEE 6063/3 2P10S375001
COMMODITY :SEAMLESS STEEL LINE PIPE WITH BEVELLED ENDS
STANDARD :DNV SMLS 450 D
SPECIFICATION :TSL-3593R4. TSL-3594R1 O. D. :114. 3mm W. T. :11. 1mm LENGTH:MIN. 12. 0m MAX. 12. 4m QUANTITY:3pcs.
MILL WORK NO. :BYYF3536 TOTAL LENGTH:36. 91m MASS:1043kg

HEAT NO. :J2L9792
PRODUCTS PCS. :3

HEAT TREATMENT :QUENCHED & TEMPERED

CHEMICAL COMPOSITION (%)

		*1	C	Si	Mn	P *3	S *3	Cu	Cr	Ni	Mo	Ti	V	Nb	B *4	N *3	*TL *3	*V1	*PCM	*A3 *2	*CEQ
SPEC. MIN.	PIPE	R	-	-	-	-	-	-	-	-	-	-	-	-	-	-	-	-	-	2	-
MAX.	NO.	R	12	45	165	20	10	35	30	30	15	6	9	5	5	12	60	15	20	-	38
HEAT NO. J2L9792		L	6	34	131	12	1	2	17	2	7	1	0	2	1	5	42	3	15	8	33
	300001	P	6	32	130	12	1	1	17	2	8	1	0	3	1	5	40	4	15	8	33
	300002	P	7	35	130	12	1	1	17	2	7	1	0	2	2	5	43	3	16	9	34

*1 R:LADLE & PRODUCT ANALYSIS L:LADLE ANALYSIS P:PRODUCT ANALYSIS *2:X1 *3:X1000 *4:X10000 OTHER:X100
*TL:Total Al *V1:Nb+V+Ti *PCM:C+Si/30+(Mn+Cu+Cr)/20+Ni/60+Mo/15+V/10+5B *A3:Total Al/N
*CEQ:C+Mn/6+(Cr+Mo+V)/5+(Cu+Ni)/15

TENSILE TEST

		*1 *2	YS *3		TS *3		EL %	YR %
SPEC. MIN.	PIPE	L B	M	450	M	535	21	-
MAX.	NO.	L B	M	570	M	655	-	93
HEAT NO. J2L9792	300001	L B	M	534	M	597	36	90

TYPE OF SPECIMEN:STRIP 25. 4mm WIDTH *1 SAMPLING DIRECTION L:LONGITUDINAL *2 SAMPLING POSITION B:BASE METAL
*3 UNIT M:MPa GAUGE LENGTH:50. 8mm KIND OF YS:0. 5% EXTENSION UNDER LOAD

IMPACT TEST (+2. 0°C 2mm V-Notch 10X6. 70)

		*1 *2	*3 *4	[1]	[2]	[3]	AVG	*3 *4	[1]	[2]	[3]	AVG
SPEC. MIN.	PIPE	T B	E J	*5	54		67	S %	*6	-		-
MAX.	NO.	T B	E J		-		-	S %		-		-
HEAT NO. J2L9792	300001	T B	E J	218	259	218	232	S %	100	100	100	100

WE HEREBY CERTIFY THAT THE MATERIAL DESCRIBED HEREIN HAS BEEN MADE IN ACCORDANCE WITH THE RULES OF THE CONTRACT.

Intertek
☑Reviewed
☐Witnessed
Initial:

Figure 1 The certificate shows the dimensions, chemical composition and mechanical properties of the pipes used in this research study.

APPENDIX-C : CALCULATION OF BENDING MOMENT IN 4 POINT BEND TEST

Outer Diameter of pipe, D

$$D := 114.3\text{mm}$$

Thickness of pipe wall, t

$$t := 11\text{mm}$$

Inner diameter of pipe, d

$$d := (D - 2t)$$

$$d = 92.3\cdot\text{mm}$$

Length of pipe Specimen, L

$$L := 730\text{mm}$$

Moment of Inertia of pipe, I

$$I := \frac{3.14\cdot\left(D^4 - d^4\right)}{64}$$

$$I = 4.813\times 10^6\cdot\text{mm}^4$$

Distance of outermost fibre, y

$$y := \frac{D}{2}$$

$$y = 57.15\cdot\text{mm}$$

Yield Stress of API X-65, σ_{yield_stress}

$$\sigma_{yield\_stress} := 540\frac{N}{\text{mm}^2}$$

Required stress at the outermost fibre of pipe, σ

$$\sigma := 300\frac{N}{\text{mm}^2}$$

Bending Moment required to generate by using equation of pure bending,M

$$M := \frac{(\sigma\cdot I)}{y}$$

$$M = 2.527\times 10^7\cdot N\cdot\text{mm}$$

Distance from support to force, b

$$b := 275\text{mm}$$

Applied Force F at one load point,

$$F_{applied} := \frac{(M \cdot 2)}{b}$$

$$F_{applied} = 183.752 \cdot kN$$

Total Load applied by clamp head, F_{total}

$$F_{total} := 2 \cdot F_{applied}$$

$$F_{total} = 367.504 \cdot kN$$

Area of Strip support

$$A := 4.5 \cdot 10^{-3} m^2$$

Pressure at one load point,

$$P := \frac{F_{applied}}{A}$$

$$P = 40.834 \cdot MPa$$

APPENDIX-D

The FEM simulation shows the linearly varying stress gradient generated along the pipe wall thickness by two fusion weld passes. The welding parameters are discussed in Section 3.4.2.

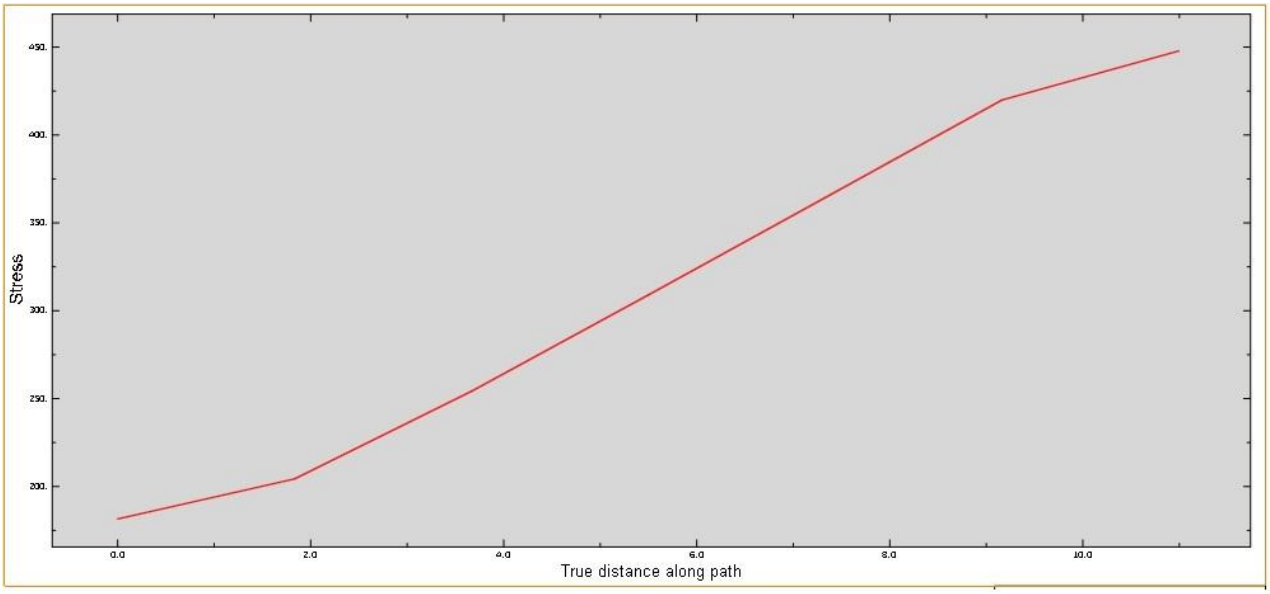

Figure 1 Figure shows the variation of residual stress gradient along pipe wall thickness.

APPENDIX - E

All the plots made by using optical measurements for all test conditions are attached in this Appendix.

- ### Test Condition 1: Pipe Specimens Without Residual Stress

The following graphs are plotted to study the crack propagation behaviour in pipe specimens without residual stresses. Optical measurements taken during fatigue tests are used to plot the graphs.

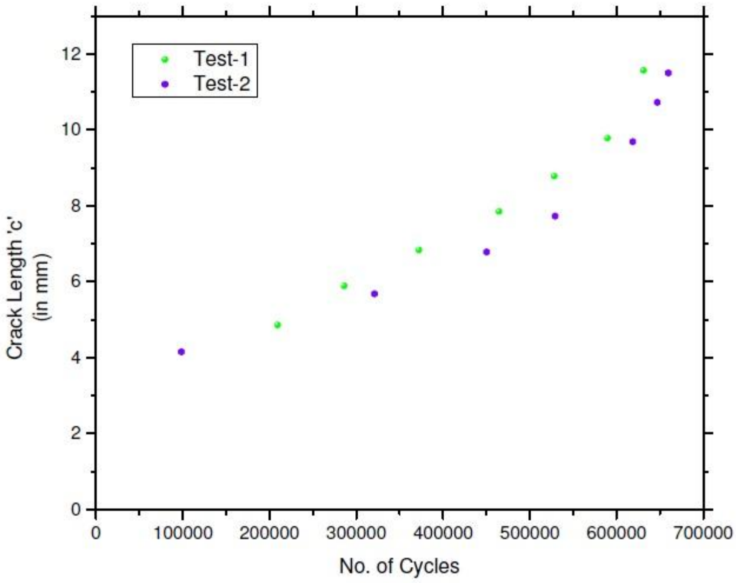

Figure 1 Figure shows crack length growth(c) in pipe specimens without residual stress

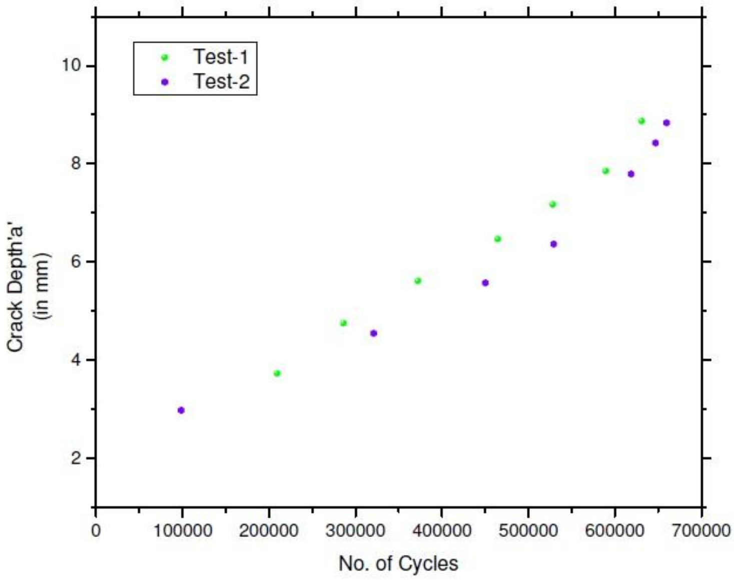

Figure 2 Figure shows crack depth growth(a) in pipe specimens without residual stress

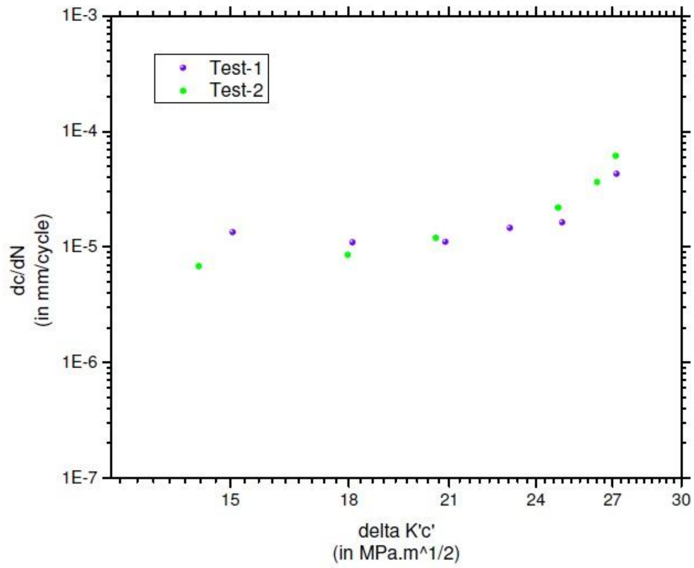

Figure 3 Figure shows Crack length growth rate (dc/dN) in pipe specimens without residual stress

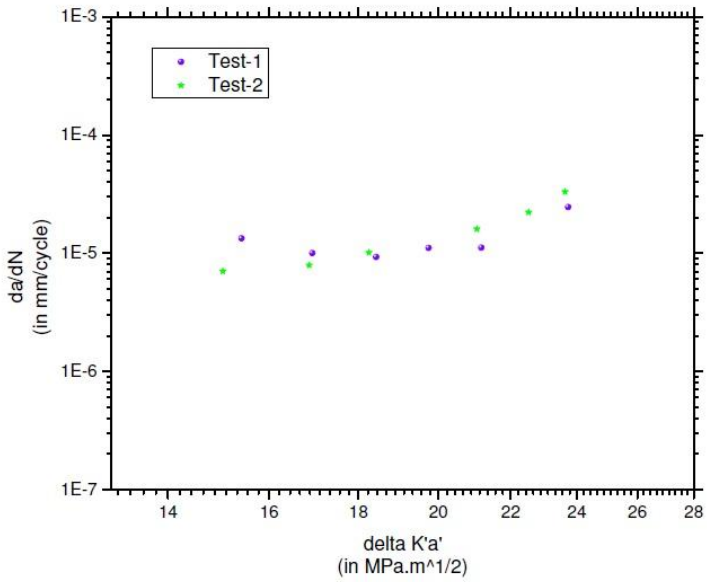

Figure 4 Figure shows Crack depth growth rate (da/dN) in pipe specimens without residual stress

- ## Test Condition 2: Pipe with Residual Stress

The following graphs are plotted to study the crack propagation behaviour in pipe specimens with residual stresses. Optical measurements taken during fatigue tests are used to plot the graphs.

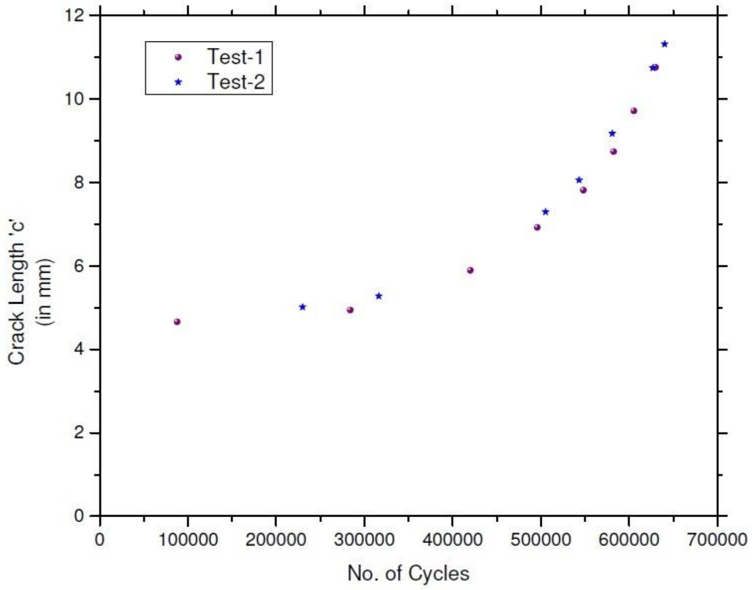

Figure 5 Figure shows Crack Length growth in pipe specimens with residual stress

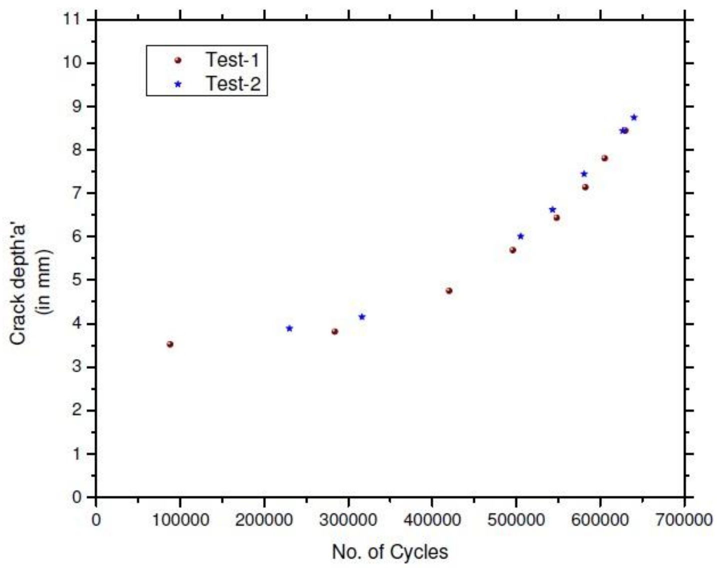

Figure 6 Figure shows Crack depth growth in pipe specimens with residual stress

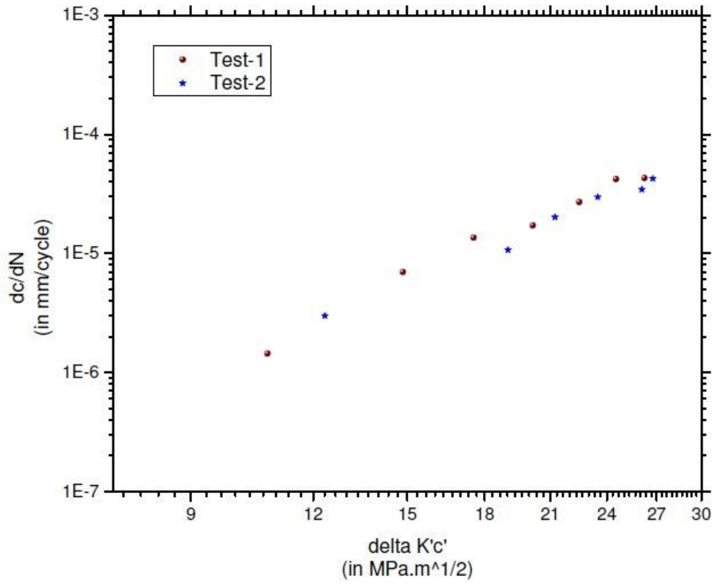

Figure 7 Figure shows Crack length growth rate (dc/dN) in pipe specimens with residual stress

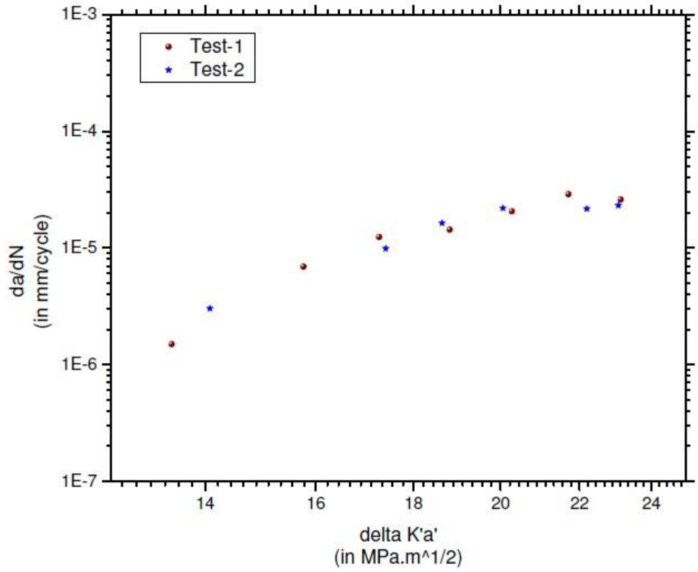

Figure 8 Figure shows Crack depth growth rate (da/dN) in pipe specimens with residual stress

- **Test Condition 3 - Strip Specimens**

The graph shows the crack growth rate(dc/dN) of 3SENB fatigue tests for strip specimens.

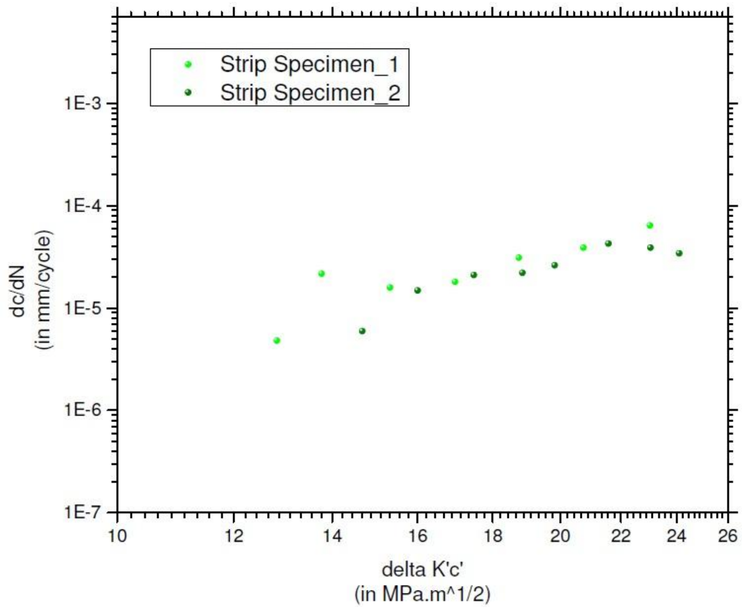

Figure 9 Figure shows crack length growth rates (dc/dN) for strip specimens

- **Comparison Of Crack Propagation Behaviour Between Pipe Specimens For both Test Conditions**

Following graphs are plotted to compare the crack propagation behaviour between pipe specimens of two test conditions.

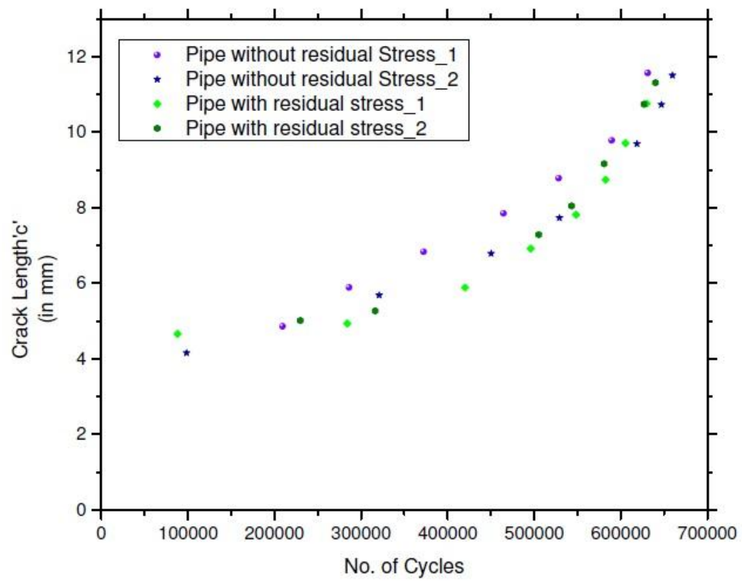

Figure 10 Figure shows the comparison for crack length(c) growth for both test conditions

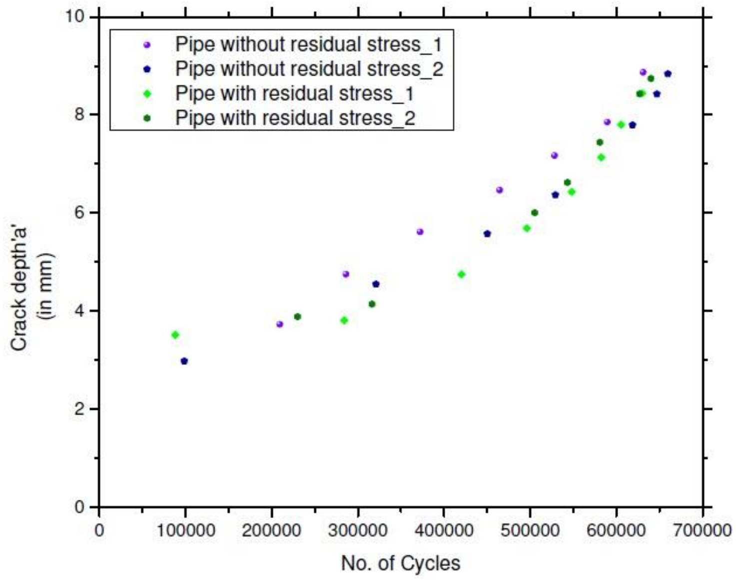

Figure 11 Figure shows crack depth(a) growth comparison for both test conditions

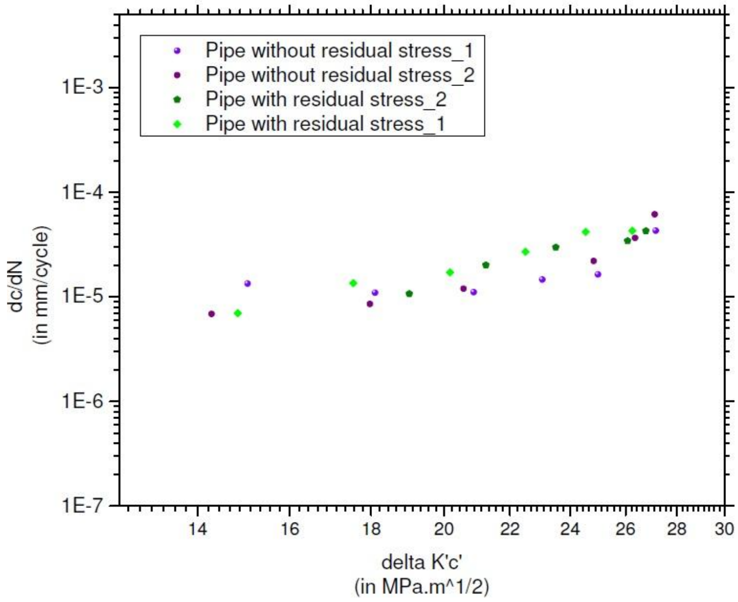

Figure 12 Figure shows crack length growth rate (dc/dN) for all pipe specimens

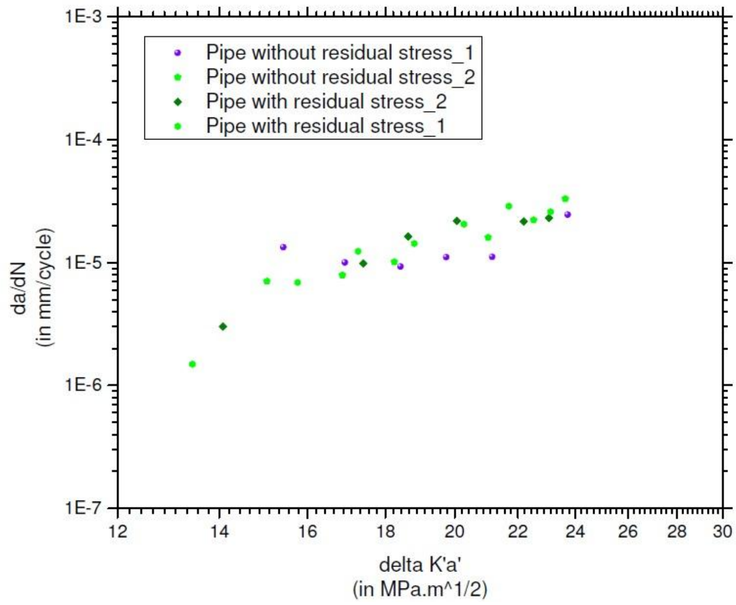

Figure 13 Figure shows crack growth rates (da/dN) for all pipe specimens

- **Comparison Of Crack Length Growth Rates Between Pipe Specimens And Strip Specimens.**

Crack length growth rates(dc/dN) are compared for strip specimens and pipe specimens to study the effect of scale on fatigue crack growth behaviour in structures as shown in Figure 14.

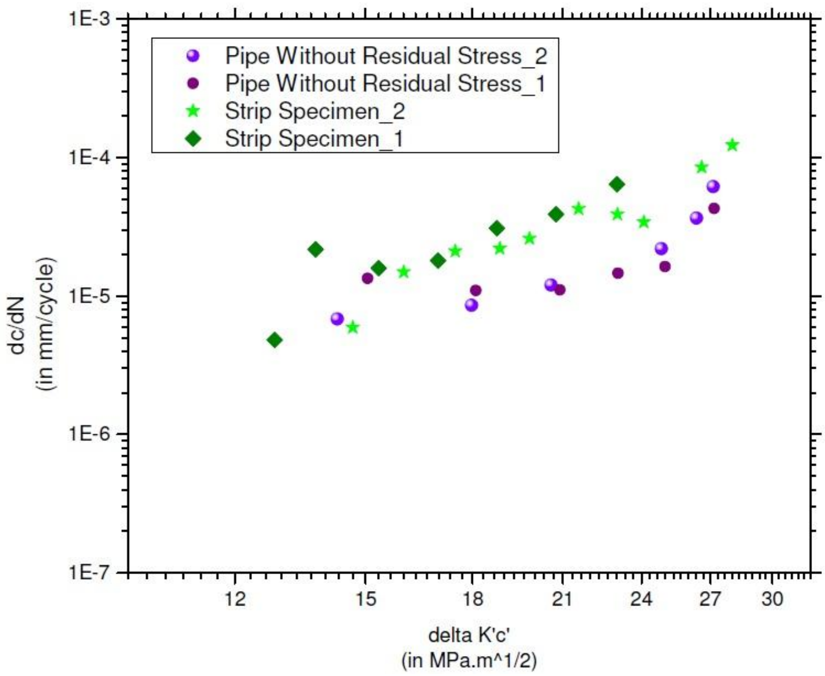

Figure 14Comparison of crack length growth rates between pipe and strip specimens